Division of Solid Mechanics

ISRN LUFTD2/TFHF- -06/5121- -SE (1-75)

VERIFICATION OF FE-MODEL FOR GASKET COMPRESSION

Master Thesis by

Björn Johansson
Oscar Järdhage

Supervisors

Paul Håkansson, Div. of Solid Mechanics, LTH
Anders Lüning, Alfa Laval Lund AB

Copyright © 2006 by Div. of Solid Mechanics (LTH),
Alfa Laval Lund AB,
Björn Johansson and
Oscar Järdhage
Printed by Media Tryck, Lund, Sweden.

For information, address:
Division of Solid Mechanics, Lund University, Box 118, SE-221 00 Lund, Sweden.
Homepage: http://www.solid.lth.se

Preface

This project is the master thesis for the degree in Master of Science in Mechanical Engineering at Lund Institute of Technology. The project was performed within the Division of Solid Mechanics and took place at Alfa Laval Lund AB, during the period of October 2005 to April 2006. Our supervisors were M.Sc. Anders Lüning, Alfa Laval Lund AB, and Lic. Eng. Paul Håkansson, Division of Solid Mechanics, LTH.

We would like to express our gratitude to Anders Lüning and Manager Michael Schanner, for giving us the possibility to perform our master thesis and for a great time at Alfa Laval. We would like to specially thank Anders Lüning for all kind of help and by making this master thesis to a great experience. We would also like to thank Paul Håkansson for always taking the time for a discussion and for giving us valuable advices. For the help with the experimental test in the laboratory of Solid Mechanics, we would like to thank laboratory engineer Zivorad Zivkovic.

Lund, april 2006

Oscar Järdhage and Björn Johansson

Abstract

For manufacturing companies it is important to have an efficient developing process. With the high-performance computer of today, FE-analyses have become an important tool in this process. The great advantage with this computer-based developing is that without having produced any prototypes or manufacturing tools the product can still be analysed. Producing prototypes are often very expensive and is delaying the developing process. Alfa Laval Lund AB is interested to continuously get a more efficient developing process and therefore increase their use of FE-analyses. Instead of designing by formulas, Alfa Laval Lund AB now wants to use FE-models to a larger extent. The reason for this is to achieve a description of the reality for the plate heat exchanger (PHE) in the best possible way and thereby to be able to minimise the dimensions of the pressure carrying components. In this project the reaction forces from the rubber gasket in the PHE is the component to be analysed.

This project is the initial step in the creation of a gasket table that will be used for the designing of PHE. Experimental tests have been performed at Alfa Laval Lund AB and at Lund University, Faculty of Engineering (LTH), to obtain the gasket forces for a compression process. The test specimens were cut out pieces from a PHE, including two plates and a rubber gasket. The purpose of this project was to create a theoretical model in the commercial Finite element program ANSYS, which describes the gasket forces in a realistic way compared to the experimental tests. To secure that this model was reliable, two different gasket geometries and material types were used.

The FE-model shows a good comparison to the tests up to a certain level of deformation. When the plates are enclosing the gasket, the FE-model becomes much stiffer than the tests. The reason for this behaviour can be addressed to the material parameters, which might not fully represent the compression process. This indicates that the model at hand is relatively good and useful.

The test specimen had a periodic symmetry, which made it possible to use symmetry conditions for the FE-model. In order to further reduce analyse time, an even smaller model was tested in ANSYS. As the boundary conditions for this model were difficult to find, a combination of different boundary conditions had to be analysed. In the range for which the FE-model represented the tests, the smaller model also showed good comparison, which makes the use of this smaller model a good indicator of the behaviour of the forces.

Contents

Chapter 1

Introduction

1.1 Short presentation of Alfa Laval

Alfa Laval is a global company, where Tetra Laval BV is the largest owner of the shares. The main office is located in Lund and Alfa Laval employs more than 9000 people world wide. Alfa Laval's operations are based on leading global positions within the three technologies: heat transfer, separation and fluid handling. One of Alfa Laval's greatest strengths is its global coverage. The company sells its products in approximately 100 countries.

Alfa Laval Lund AB, named Alfa Laval in the following of this thesis, develops and produces plate heat exchangers. The company is world leading and offers a wide range of different kinds of plate heat exchangers for their customers.

1.2 Background

For manufacturing companies it is important to have an efficient developing process. With the high-performance computer of today, FE-analyses have become an important tool in this process. The great advantage with this computer-based developing is that without having produced any prototypes or manufacturing tools the product can be analysed. Producing prototypes are often very expensive and delays the developing process. It should be mentioned that prototypes are important in the developing process, but that the advantage with FE-analyses is that less prototypes are needed. Alfa Laval is of course interested to continuously get a more efficient developing process and therefore increase their use of FE-analyses.

The plate heat exchanger (PHE) is considered as a pressure vessel, and therefore designed according to a pressure vessel code. When designing the PHE one have to consider for loads such as inner- and outer pressure, gasket forces, nozzle loads from connection pipes and loads of inertia, e.g. earthquake. Instead of designing by formulas, Alfa Laval now wants to use FE-models to a larger extent. The reason for this is to achieve a description of the reality in a better way for the PHE, and to minimise the dimensions of the pressure carrying components. To avoid failure of the PHE and to minimize conservatism, an accurate analysis of the true gasket force is necessary.

1.3 Objective

The purpose of this project is to create a theoretical model in the FE program ANSYS, which describes the gasket force in a realistic way. The forces will be measured for a PHE that is not exposed to any pressure and temperature loads. This project will be the initial step in the creation of a gasket table that will be used for the designing of PHE.

Alfa Laval has created test equipment for measuring gasket forces. In this test equipment, cut out pieces of a gasket and plates can be placed to simulate the compression of a gasket.

The test will be conducted so that the gasket is compressed until the two plates are nearly in metallic contact with each other. The test shall be repeated in a theoretical FE-model in ANSYS, based on real geometries and given parameters.

The major purpose of this work is to investigate if ANSYS is capable of this kind of problems and how it should be modelled, along with a verification of the parameters. The reaction forces from the experimental tests should be comparable with the theoretical model. To secure that the model in ANSYS is reliable, tests will be made with a second geometry and material properties. Experimental tests will also be made with this geometry.

The problem at hand is non-linear in terms of the material, boundary conditions and geometry and therefore theory for dealing with non-linearity have to be used. For material non-linearity the strain energy density functions will be used. The non-linear behaviour will be solved with help of the Newton-Raphson method.

1.4 Model

The geometric model used in the analyses was made by Alfa Laval by means of CAD-software, see Figure 1.1. This figure shows a cut out part of a rubber gasket placed between two corrugated plates, located at the vertical groove of the plate heat exchanger. Two different gasket geometries will be used in the FE-simulations and experimental tests. For geometry 1, Nitrile based rubber will be evaluated. Geometry 2 will be evaluated with both Nitrile based rubber and EPDM. The difference between geometry 1 and geometry 2 is that the height of geometry 2 is larger than for geometry 1.

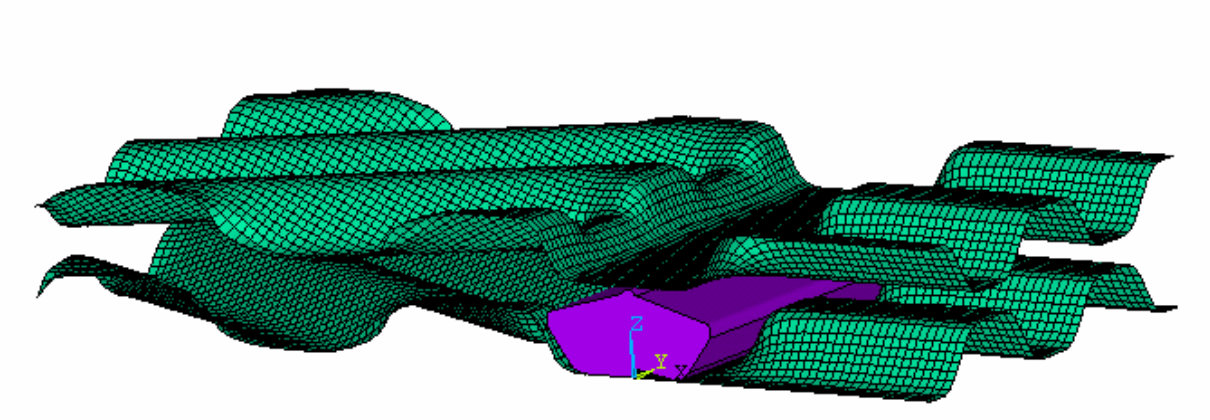

Figure 1.1: *Original plates with gasket geometry 1*.

1.4.1 Limitations

When making the tests and simulations only a small cut out piece of the plates and gasket are evaluated. Boundary conditions are therefore different than if a simulation would have been made on a complete plate heat exchanger. The purpose of this project is to compare results from tests of the small cut out piece and simulations in ANSYS, and not to create a simulation of the complete PHE.

The model analysed in ANSYS has a shorter length than the cut out piece used in the tests on Alfa Laval. The results from the simulations in ANSYS are therefore linearly extrapolated, for comparison to the real made tests.

The FE-model will not take any rate dependency for the rubber into consideration. The experimental tests to be compared with the FE-model will therefore be carried out with low speed of deformation.

Chapter 2

The plate heat exchanger

This text is based on [7], which is a summary of booklets published by Alfa Laval, containing some basic information about plate heat exchangers, [1].

Many industries use PHE in their work. The PHE is available for different kinds of application and the companies vary from industries such as the chemical process industry, offshore platforms, sugar plants, pulp and paper plants to breweries, food and dairy plants, refrigeration plants and more.

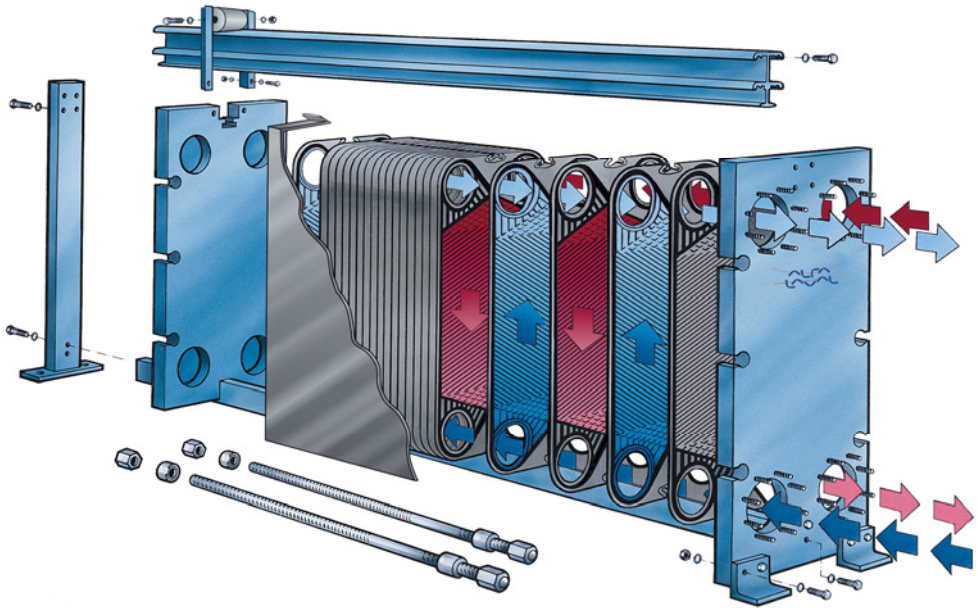

Figure 2.1: *The heat transfer area in the plate heat exchanger consists of a pack of thin corrugated metal plates*.[1]

A PHE is an assembly of several components, which can be seen in Figure 2.1. The corrugated plates are placed between two pressure plates. This package of plates are carried by a bar that is connected to bar construction and compressed by bolts. For the sealing function a rubber gasket is often used. Pipes connected to the PHE transport the two fluids that will undergo the heat exchange, where fluids flow on different side of the corrugated plate. The reasons for using corrugated plates are to get turbulence in the fluids, obstruct pressure differences and to get a larger surface of heat transfer. The design of the PHE, number and size of the plates, are of course dependent on which capacity that is requested. The corrugated plates are manufactured through a cold-forming process. The most common used materials are stainless steel, titanium and nickel alloys. For the rubber gasket several types of elastomers are possible such as NBR, EPDM, Viton and Neoprene.

The gasket is to be considered as an accessory part in the PHE, and its lifetime is dependent on the process. The parameter that affects this lifetime the most is the process temperature. Small differences around the maximal allowed temperature could also have large impact on the lifetime. There are three different ways to fasten the gasket to the corrugated plate, such as gluing, taping or with clip-on. The choice of gasket and fasten technique depends on the specific range of application. When the PHE is assembled the corrugated plates are pressed into contact to each other, but under operation this contact disappear and the gasket has the sealing function.

Chapter 3

Introduction to rubber material

This chapter describes the molecular structure and manufacturing process for rubber, as well as the general mechanical properties. A short description will be given for the two different rubber gaskets analysed in this project. The theory for finding the proper material parameters will be discussed in Appendix A. In this chapter the text is based on the thesis *Modelling of Elasticity and Damping for Filled Elastomers* written by Per-Erik Austrell [3].

3.1 Molecular structure and manufacturing process

Rubber or elastomers are the names for a group of material with the same mechanical properties and rather like molecular structure. This group of material are polymers based on different kinds of organic substances, either natural or synthetic, all with long molecular chains. To create rubber, the raw material must undergo a process called vulcanization, where the purpose is to create links between the long molecular chains. Before this process the material is plastic but with the linking the material get a more stable and solid molecular structure. This is a chemical process and is performed by adding sulfur to the raw material, thereafter the mixture is heated up to a certain temperature where the linking process starts. There is a possibility to increase the stiffness of the rubber, which is done by adding small particles, fillers, to the raw material before the vulcanization process. These particles can for example be carbon with a size of $20n\text{m} - 50\,\mu\text{m}$, called *carbon black*. Under the vulcanization process this stiffness-boosted mixture creates cross-links between the filler particles and the long molecular chains. A molecular structure of a carbon black filled rubber is shown in Figure 3.1. The polymer chains are shown as solid lines and cross links are shown as dashed lines.

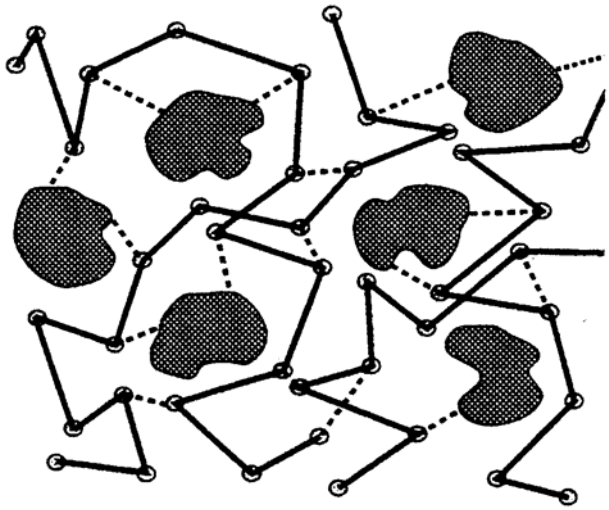

Figure 3.1: *The molecular structure for a carbon black filled rubber vulcanizate. Dashed lines are cross links and solid lines are the polymer chains.* [3]

3.2 Mechanical properties

Rubber material has two important properties, the possibility to undergo large elastic straining and also to damp vibration. To begin with the elastic property, this is due to the long and tangled molecular chains. Under loading they have the possibility to rotate and thereby orientate themselves in the loading direction. With this feature the rubber has the possibility to be elastic strained several hundred percent. The damping properties can be referred to the phenomenon called *hysteresis*, and can be seen in Figure 3.2. The loading and un-loading paths in Figure 3.2 are different which indicates that the rubber is not perfectly elastic. The area between these two paths represents the energy loss for this loading and un-loading procedure. This energy loss is mainly dissipated as heat and this effect is the one causing the damping property for rubber.

When an unstrained rubber specimen undergoes a cyclic loading to a specific stretch, the needed force will gradually decrease and reach a steady state after three to five cycles. Under cyclic loading the rubber network changes and the cross-links collapse, which causes the described phenomenon called *Mullins effect* and can be seen in Figure 3.2. In this project, no aspects of Mullin's effect will be taken into consideration, as the experimental tests are made with new rubber specimens.

Rubber material is to be considered as nearly incompressible due to the large difference between the bulk- and shear modules. For the mentioned carbon black filled rubber this bulk modulus is 2000 times larger than the shear modulus. For many applications complete incompressibility is a good assumption.

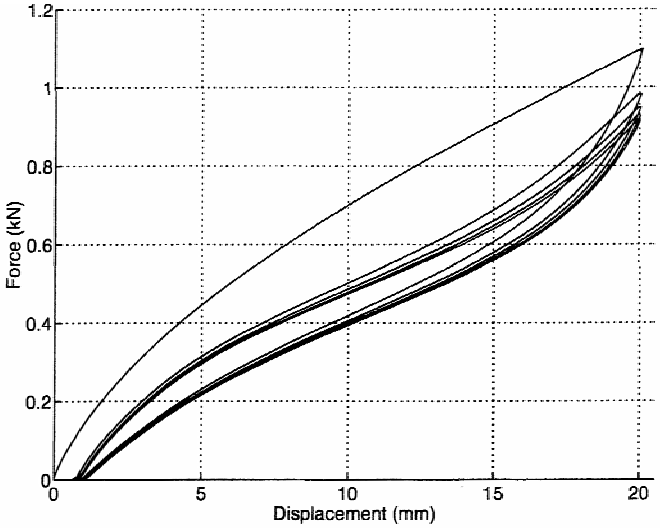

Figure 3.2: *Force-displacement relations for a rubber vulcanizate exposed to cyclic loading.*[3]

Another important aspect of rubber is the *viscous* effects. When, as for this project, a rubber specimen is exposed to compression, the stresses in the material are time dependent. For a high speed of compression the initial stresses becomes larger than for a lower speed. If the compression is held at a specific level, the stresses in the material will decrease for a period of time, until it reaches a converged value. This behaviour is called *relaxation*. For the opposite case, where the stress is held constant, the strains in the material will increase causing *creep*. The viscoelastic model is assumed to be composed of non-linear springs and a linear dashpot, see Figure 3.3.

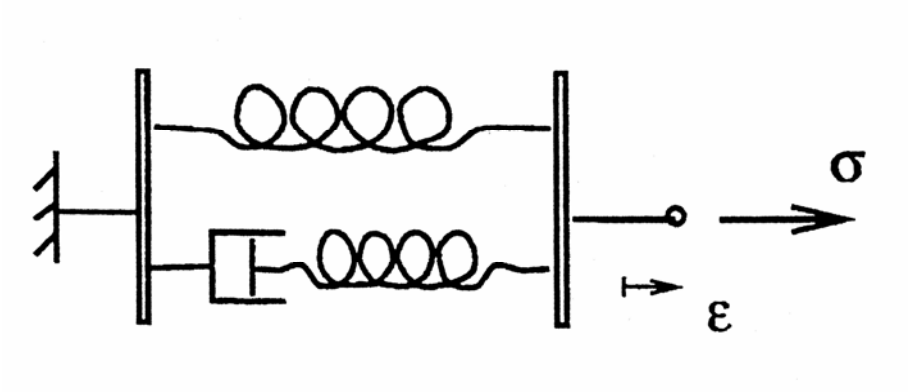

Figure 3.3: *Non-linear viscoelastic model.* [3]

3.3 Short description of the gasket materials

In a PHE from Alfa Laval, two different rubber gaskets are mainly used. These are Nitrile Based Rubber (NBR) and Ethylene Propylene Rubber (EPDM).

NBR is a suitable rubber for applications requiring resistance to petroleum-based fluids. Although there are other rubbers that have higher resistance, NBR is mostly used because of its low price. It has low permeability to gases, and can resist temperatures up to $100\,°C$. It is also economical to compound and produce. There are some drawbacks such as poor resistance to outdoor weathering without special compounds and flammability with toxic gases. NBR are most common rubber for oil and fuel resistance components such as gaskets and seals, membranes, hoses and cable mantles.

EPDM was originally developed for tyre applications but became eventually more widely used because of its suitable for outdoor use. EPDM is one of the most water resistant types of rubber and can also resist water-based chemicals. The structure is very inert and remains stable over long periods of time. The rubber can resist temperatures up to $120\,°C$ for several months. The disadvantage of EPDM is the low resistance to oil and oil based products and the compression set is not so good without special compounding. EPDM is used in many different applications, such as O-rings, gaskets, door- and window seals, cable insulation, roller-coating, conveyor belts, hoses, bellows and clothing.

Chapter 4

Non-linear theory and FE-implementation

This chapter will begin with the theory for the problem at hand and will end up with the numerical approach for solving the problem. The problem is non-linear in terms of geometry, material and boundary conditions. The first part will describe the theory for dealing with the geometric non-linearity, by defining proper stresses, virtual work and strains. Thereafter the material non-linearity is described by the so called strain energy function. Here, the Yeoh-model is used as strain energy function. The boundary non-linearity in this problem is defined by the contact and friction. This will not be included in this chapter, but is briefly described in chapter 6.

Finally, the numerical implementation, the finite element method, and due to the non-linearity, the Newton-Raphson iteration method will be described.

4.1 Geometric non-linearity

For a body exposed to some kind of force, the equilibrium equation is established for the deformed shape of the body. In case of small deformation this deformed shape is approximated with the un-deformed and known shape, but for large deformation the deformed shape is unknown and needs to be considered.

In this section the theory for handling this type of geometric problem will be described. It will start with defining large deformation. Thereafter the *Cauchy-stresses* which yield for the current configuration will be described. In ANSYS a so called Updated Lagrangian formulation is handling problems including large deformation, which uses the current configuration and therefore Cauchy stresses are used. These Cauchy stresses are based on the *second Piola-Kirchhoff* stresses which yield for the initial configuration. It is therefore necessary to show how the second Piola-Kirchhoff stresses are converted to the Cauchy-stresses, by use of the virtual work equation.

For a more elaborate description of the finite displacement theory the reader is referred to [6].

4.1.1 Large deformation and strains

Figure 4.1 shows a body in the un-deformed state and the current deformed state. A set of orthogonal unit base vectors $\mathbf{i}_1, \mathbf{i}_2, \mathbf{i}_3$ is introduced forming a Cartesian coordinate system. The initial position vector for the un-deformed body can be written in component form as

$$\mathbf{x}_0 = x_1^0 \mathbf{i}_1 + x_2^0 \mathbf{i}_2 + x_3^0 \mathbf{i}_3 . \tag{4.1}$$

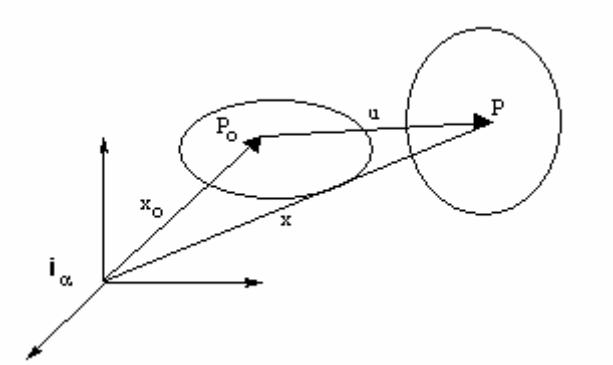

Figure 4.1: *Displacement* **u** *from initial configuration* $\mathbf{x}_0$ *to current configuration* $\mathbf{x}$.

With a displacement of the body, by the displacement vector **u**, the new position is defined as

$$\mathbf{x} = \mathbf{x}(\mathbf{x}_0) = \mathbf{x}_0 + \mathbf{u} \tag{4.2}$$

To be able to measure strain, infinitesimal lengths must be used. This is because strain is a point property for a continuum. In the initial configuration a vector $d\mathbf{x}_0$ with length ds_0 is considered. After the deformation, this vector is defined by $d\mathbf{x}$, Figure 4.2. The coordinates for $d\mathbf{x}$ is defined by partial derivatives of (4.2) and $d\mathbf{x}_0$ as

$$d\mathbf{x} = \mathbf{F}\, d\mathbf{x}_0 \tag{4.3}$$

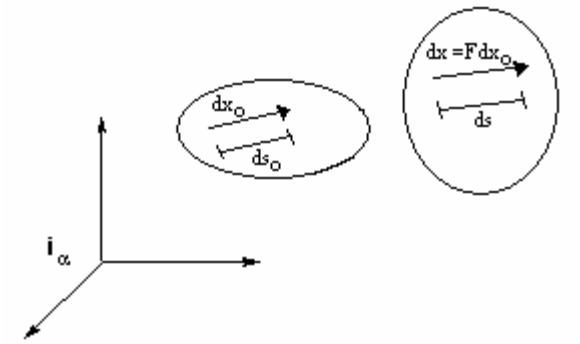

Figure 4.2: *Motion of infinitesimal vector* $d\mathbf{x}$.

where **F** is the *deformation gradient tensor*

$$\mathbf{F} = \begin{bmatrix} \partial x_1 / \partial x_1^0 & \partial x_1 / \partial x_2^0 & \partial x_1 / \partial x_3^0 \\ \partial x_2 / \partial x_1^0 & \partial x_2 / \partial x_2^0 & \partial x_2 / \partial x_3^0 \\ \partial x_3 / \partial x_1^0 & \partial x_3 / \partial x_2^0 & \partial x_3 / \partial x_3^0 \end{bmatrix} \tag{4.4}$$

This tensor can be expressed with a unit tensor and the partial derivatives concerning the actual displacement in (4.2) as

$$\mathbf{F = I + D} \tag{4.5}$$

Where the tensor **D** is the *displacement gradient tensor*

$$\mathbf{D} = \begin{bmatrix} \partial u_1/\partial x_1^0 & \partial u_1/\partial x_2^0 & \partial u_1/\partial x_3^0 \\ \partial u_2/\partial x_1^0 & \partial u_2/\partial x_2^0 & \partial u_2/\partial x_3^0 \\ \partial u_3/\partial x_1^0 & \partial u_3/\partial x_2^0 & \partial u_3/\partial x_3^0 \end{bmatrix} \tag{4.6}$$

With the vectors $d\mathbf{x}_0$ and $d\mathbf{x}$ defining the initial and deformed state, the *Green strain* ε_G is expressed in the following way

$$\varepsilon_G = \frac{ds^2 - ds_0^2}{2\,ds_0^2} = \frac{d\mathbf{x}^T d\mathbf{x} - d\mathbf{x}_0^T d\mathbf{x}_0}{2\,ds_0^2} \tag{4.7}$$

By use of (4.3) this expression can be reformulated to

$$\varepsilon_G = \frac{d\mathbf{x}_0^T}{ds_0} \tfrac{1}{2}(\mathbf{F}^T\mathbf{F} - \mathbf{I}) \frac{d\mathbf{x}_0}{ds_0} \tag{4.8}$$

The first and last term defines the direction for the vector in the initial state, and the middle term is defined as the *Green strain tensor,*

$$\mathbf{E} = \tfrac{1}{2}(\mathbf{F}^T\mathbf{F} - \mathbf{I}) = \tfrac{1}{2}(\mathbf{D} + \mathbf{D}^T) + \tfrac{1}{2}\mathbf{D}^T\mathbf{D} \tag{4.9}$$

The components for the Green strain tensor are found by use of (4.6), and can now be written as

$$E_{\alpha\beta} = \frac{1}{2}\left(\frac{\partial u_\alpha}{\partial x_\beta} + \frac{\partial u_\beta}{\partial x_\alpha}\right) + \frac{1}{2}\frac{\partial u_\gamma}{\partial x_\alpha}\frac{\partial u_\gamma}{\partial x_\beta} \tag{4.10}$$

The Green strain tensor is a symmetric matrix and each component is a sum of a linear and quadratic term. For the case of small deformation the quadratic term is negligible for the strain value, which shows that the Green strain corresponds to the theory of small deformation. To be able to establish the principle of virtual work later in this chapter, the variation $\delta\mathbf{E}$ is needed. From (4.9) this variation is found as

$$\delta\mathbf{E} = \tfrac{1}{2}(\mathbf{F}^T\delta\mathbf{D} + \delta\mathbf{D}^T\mathbf{F}) \tag{4.11}$$

The corresponding component form is

$$\delta E_{\alpha\beta} = \tfrac{1}{2}\left(\frac{\partial x_\gamma}{\partial x_\alpha^0}\frac{\partial(\delta u_\gamma)}{\partial x_\beta^0} + \frac{\partial(\delta u_\gamma)}{\partial x_\alpha^0}\frac{\partial x_\gamma}{\partial x_\beta^0}\right) \tag{4.12}$$

Later in this chapter two other strain measures will be used and are therefore here presented. These strain measures are both based on the deformation gradient tensor **F**, and are the *left Cauchy-Green* deformation tensor $\mathbf{B} = \mathbf{F}\mathbf{F}^T$ and the *right Cauchy-Green* deformation tensor $\mathbf{C} = \mathbf{F}^T\mathbf{F}$.

4.1.2 Cauchy-stress

Internal forces in a body can accrue by several factors, where external loads are common. These internal loads are defined by stresses, which are measured as force per unit area.

A reaction force $\Delta\mathbf{P}$ is acting on a arbitrary cross-section area ΔA, defined by unit vector **n**, see Figure 4.3.

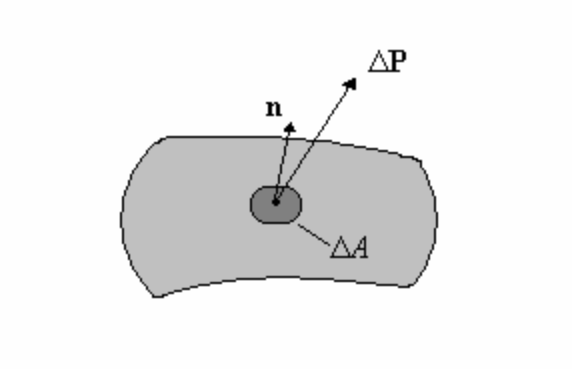

Figure 4.3: *Forces on a cross-section area.*

If ΔA approaches zero the ratio $\Delta\mathbf{P}/\Delta A$ defines the traction vector for the point where the force is acting,

$$\mathbf{t} = \frac{d\mathbf{P}}{dA} \tag{4.13}$$

This traction vector **t** includes the normal and shear stresses acting in the point for the specific cross-section. To get a complete description of the stress state in the point, three orthogonal cross-sections through the point has to be carried out. The stress state is completely described by the Cauchy-stress tensor σ. Due to the requirement of moment equilibrium σ is symmetric according to [8].

$$\sigma = \begin{bmatrix} \sigma_{xx} & \sigma_{xy} & \sigma_{xz} \\ \sigma_{xy} & \sigma_{yy} & \sigma_{yz} \\ \sigma_{xz} & \sigma_{yz} & \sigma_{zz} \end{bmatrix} \tag{4.14}$$

Where the traction vector **t** is,

$$\mathbf{t} = \sigma\mathbf{n} \text{ or } t_\alpha = \sigma_{\alpha\beta} n_\beta \tag{4.15}$$

4.1.3 Stresses for geometrical non-linearity

It is now time to define the relation between the Cauchy-stresses and the second Piola-Kirchhoff stresses, by use of the virtual work equation. The first step is to establish the equation for the Cauchy-stresses, thereafter for the second Piola-Kirchhoff stresses.

By considering an arbitrary part of a body, with surface forces defined by t_α and body forces defined by b_α, the equilibrium equation is here established as

$$\int_S t_\alpha \, dS + \int_V b_\alpha \, dV = 0 \tag{4.16}$$

This equilibrium equation can be reformulated by use of (4.15) and Gauss' divergence theorem to

$$\int_V (div\,\sigma_{\alpha\beta} + b_\alpha)\, dV = 0 \tag{4.17}$$

As the equation was stated for an arbitrary volume the expression within the parenthesis must fulfil the following requirement

$$div\,\sigma_{\alpha\beta} + b_\alpha = 0 \tag{4.18}$$

To establish the virtual work equation, the equilibrium equation is multiplied by an arbitrary incremental displacement δu_α, and thereby integrated over a volume *V*. By use of the Green-Gauss theorem this virtual work equation can be written, according to [6], at index notation as,

$$\int_V \delta\varepsilon_{\alpha\beta}\, \sigma_{\alpha\beta}\, dV = \int_S \delta u_\alpha\, t_\alpha\, dS + \int_V \delta u_\alpha\, b_\alpha\, dV \tag{4.19}$$

The virtual work equation with Green strain components $\delta E_{\alpha\beta}$ and the *second Piola-Kirchhoff* stresses $S_{\alpha\beta}$ is then written as,

$$\int_{V_0} \delta E_{\alpha\beta} S_{\alpha\beta} dV_0 = \int_{S_0} \delta u_\gamma t_\gamma^0 dS_0 + \int_{V_0} \delta u_\gamma p_\gamma^0 dV_0 \tag{4.20}$$

Equation (4.19) is the virtual work equation for the current configuration, while (4.20) is the same virtual work equation formulated in the reference configuration, i.e. total Lagrangian formulation. An updated Lagrangian formulation, as used in ANSYS, is obtained if the configuration continuously is updated by the new deformations that occur in the last iteration of the load step. By now considering a displacement *d***u** for the current state, the occurring strain increments can be formulated as the linear part of the Green strains, according to [6].

$$d\varepsilon_{\alpha\beta} = \frac{1}{2}\left(\frac{\partial(du_\alpha)}{\partial x_\beta} + \frac{\partial(du_\beta)}{\partial x_\alpha} \right) \tag{4.21}$$

By reformulating (4.12) with use of the chain rule of differentiation for *d***u**, the Green strain increment becomes

$$dE_{\alpha\beta} = \frac{1}{2}\left(\frac{\partial x_\gamma}{\partial x_\alpha^0} \frac{\partial(du_\gamma)}{\partial x_\lambda} \frac{\partial x_\lambda}{\partial x_\beta^0} + \frac{\partial x_\lambda}{\partial x_\alpha^0} \frac{\partial(du_\gamma)}{\partial x_\lambda} \frac{\partial x_\gamma}{\partial x_\beta^0} \right) \tag{4.22}$$

By now comparing the two strain expression (4.21) and (4.22), the relation between the Green strain increment and the linear strain increment can be formulated. As $dE_{\alpha\beta}$ is symmetric, the relation between them is written as

$$d\mathbf{E} = \mathbf{F}^T d\varepsilon \mathbf{F} \tag{4.23}$$

This also holds for the variation of $\delta\mathbf{E}$ and $\delta\varepsilon$.

The internal part in the virtual work equation (4.19) and (4.20) can now be established for both Cauchy and second Piola-Kirchhoff stresses, and the expression needs to be equal. The one with Cauchy-stresses uses the current state as reference configuration and therefore the virtual linear strain. For the second Piola-Kirchhoff stresses, which use the initial state as reference configuration, the virtual Green strain is used.

$$\int_{V_0} \delta E_{\alpha\beta} S_{\alpha\beta} dV_0 = \int_V \delta\varepsilon_{\alpha\beta}\sigma_{\alpha\beta} dV \tag{4.24}$$

The current volume is given by the triple product of the side vectors,

$$dV = \left(\frac{\partial \mathbf{x}}{\partial x_1^0} \cdot \frac{\partial \mathbf{x}}{\partial x_2^0} \times \frac{\partial \mathbf{x}}{\partial x_3^0} \right) dV_0 = \det\left(\frac{\partial x_\alpha}{\partial x_\beta^0} \right) dV_0 \tag{4.25}$$

Introducing the Jacobian determinant $J = \det(\mathbf{F})$ the volume relation is

$$dV = JdV_0 = \det(\mathbf{F}) dV_0 \tag{4.26}$$

Introduction of this relation and the strain increment relation (4.23) into the left side of (4.24) gives the following formula for the Cauchy stress,

$$\sigma = \frac{1}{J}\mathbf{F}\mathbf{S}\mathbf{F}^T \tag{4.27}$$

4.2 Material non-linearity

The PHE consists of mainly two materials, metal and rubber. Metal have a fairly linear stress-strain relationship at low strain values, but at higher strains the material yields and the response becomes non-linear and irreversible. The plates in this project are assumed to be rigid bodies, due to the large difference in stiffness between the plates and the rubber gasket. Therefore no further description will be made on this issue.

This chapter therefore serves as an introduction to non-linear elastic material models. As mentioned earlier, rubber is a highly non-linear material and therefore the simple linear elastic stress-strain relation with a constant Young's modulus, E, does not apply. For this reason it is necessary to use some other kind of mathematical model to describe the material behaviour. For modelling the rubber gasket in this project, a *hyperelastic material* model is used.

The constitutive equation for a hyperelastic material is defined as a relation between the total stress and the total strain. The strain energy plays a central role in defining the constitutive relation. Stresses are determined by derivatives of the strain energy function, giving the second Piola-Kirchhoff stresses.

A one-dimensional example will be used to illustrate how the nominal stresses can be obtained by the strain energy function. A description for the general case will be stated after the example with the non-linear elastic bar.

4.2.1 Non-linear elastic bar

A force P is acting on a non-linear elastic bar with length L and cross section area A, cf. Figure 4.4. The force causes a displacement *u* of the bar. The stretch λ is defined as the rate between the new length *l* and the original *L* as $\lambda = l / L$.

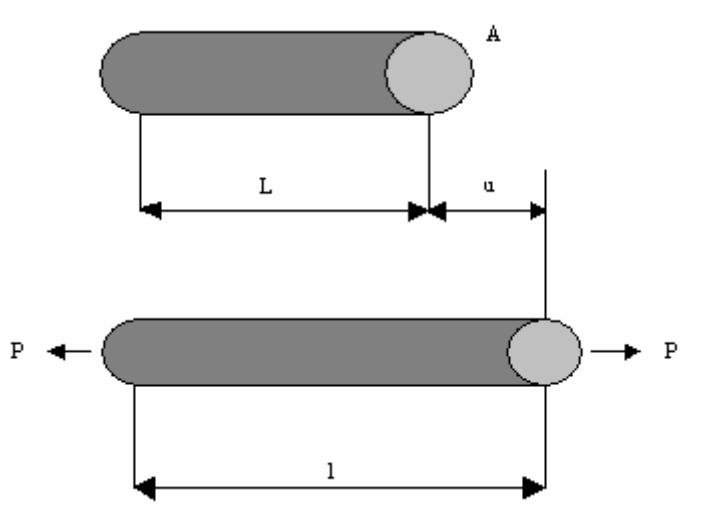

Figure 4.4: *Non-linear elastic bar loaded with a force* P.

By multiplying the strain energy density W to the original volume, the strain energy U becomes:

$$U = ALW(\lambda). \tag{4.28}$$

The incremental work done by the force P is defined as

$$Pdu = dU \tag{4.29}$$

This incremental work can also be expresses by an increment of the total strain energy

$$dU = ALdW = AL\frac{dW}{d\lambda}d\lambda \tag{4.30}$$

The displacement can be formulated as a function of the stretch λ and L as

$$u = l - L = (\lambda - 1)L \tag{4.31}$$

Differentiation of displacement function yields

$$du = Ld\lambda \tag{4.32}$$

Inserting (4.32) and (4.29) into (4.30) gives

$$PLd\lambda = AL\frac{dW}{d\lambda}d\lambda \tag{4.33}$$

Simplifying the expression gives

$$S = \frac{P}{A} = \frac{dW}{d\lambda} \tag{4.34}$$

where S is the nominal stress, i.e. force per original cross-section area, derived from the strain energy function. From this bar example it is proved that the stresses are obtained directly by deriving the strain energy function W. This holds even for the general case and this will be shown in the next section.

4.2.2 The general constitutive model

As could be seen for the non-linear elastic bar, the stresses can be obtained by deriving the strain energy function W. In this section the stresses for a hyperelastic material will be evaluated from the concept of derivation of the strain energy function. For the interested reader, a more elaborate derivation can be found in *Nonlinear Solid Mechanics, a Continuum Approach for Engineering*, written by Gerhard A. Holzapfel [5].

The strain energy function that will be derived is a function of the strain invariants I_1, I_2, I_3. These invariants are functions of the earlier described *right Cauchy-Green* deformation tensor, $\mathbf{C}$.

$$W = W\left[I_1(\mathbf{C}), I_2(\mathbf{C}), I_3(\mathbf{C})\right] \tag{4.35}$$

According to [5] the second Piola-Kirchhoff stresses can be calculated from the derivation of the strain energy function as

$$\mathbf{S} = 2\frac{\partial W(\mathbf{C})}{\partial \mathbf{C}} \tag{4.36}$$

By using the chain rule of differentiation (4.36) becomes

$$\mathbf{S} = 2\left[\frac{\partial W}{\partial I_1}\frac{\partial I_1}{\partial \mathbf{C}} + \frac{\partial W}{\partial I_2}\frac{\partial I_2}{\partial \mathbf{C}} + \frac{\partial W}{\partial I_3}\frac{\partial I_3}{\partial \mathbf{C}}\right] \tag{4.37}$$

With an isotropic material the strain invariants are defined as

$$\begin{cases} I_1 = tr(\mathbf{C}) = \lambda_1^2 + \lambda_2^2 + \lambda_3^2 \\ I_2 = \frac{1}{2}(tr(\mathbf{C})^2 - tr(\mathbf{C}^2)) = \lambda_1^2\lambda_2^2 + \lambda_1^2\lambda_3^2 + \lambda_2^2\lambda_3^2 \\ I_3 = \det(\mathbf{C}) = \lambda_1^2\lambda_2^2\lambda_3^2 \end{cases} \tag{4.38}$$

This gives the expression for the Piola-Kirchhoff stresses as

$$\mathbf{S} = 2\left[\left(\frac{\partial W}{\partial I_1} + I_1\frac{\partial W}{\partial I_2}\right)\mathbf{I} - \frac{\partial W}{\partial I_2}\mathbf{C} + I_3\frac{\partial W}{\partial I_3}\mathbf{C}^{-1}\right]. \tag{4.39}$$

To be able to transform the Piola-Kirchhoff stresses to Cauchy stresses, equation (4.27) is used. By multiplying the tensor variables $\mathbf{I}, \mathbf{C}, \mathbf{C}^{-1}$ with $\mathbf{F}$ from the left hand side and $\mathbf{F}^T$ on the right hand side, by means of the *left Cauchy-Green* deformation tensor $\mathbf{B} = \mathbf{F}\mathbf{F}^T$ this gives,

$$\mathbf{F}\mathbf{I}\mathbf{F}^T = \mathbf{F}\mathbf{F}^T = \mathbf{B}, \qquad \mathbf{F}\mathbf{C}\mathbf{F}^T = (\mathbf{F}\mathbf{F}^T)^2 = \mathbf{B}^2, \qquad \mathbf{F}\mathbf{C}^{-1}\mathbf{F}^T = (\mathbf{F}\mathbf{F}^{-1})(\mathbf{F}^{-T}\mathbf{F}^T) = \mathbf{I}$$

Which gives the Cauchy stresses as

$$\sigma = \frac{2}{J}\left[\left(\frac{\partial W}{\partial I_1} + I_1\frac{\partial W}{\partial I_2}\right)\mathbf{B} - \frac{\partial W}{\partial I_2}\mathbf{B}^2 + I_3\frac{\partial W}{\partial I_3}\mathbf{I}\right]. \tag{4.40}$$

4.2.3 The strain energy function for an incompressible material

The strain energy function for an isotropic material was described in the latter section, and is a function of the strain invariants I_1, I_2, I_3, c.f. (4.38). In the case of an incompressible material, there is no dependence on the third invariant as this expresses the volumetric change. The strain energy is therefore now only a function of the first- and second invariant and yields

$$W = W(I_1, I_2). \tag{4.41}$$

In the following of this section, the form (4.41) will be used. Due to condition of incompressibility, $I_3 = 1$ which makes it possible to eliminate one of the principle stretches in the expressions of I_1 and I_2. The third principle stretch can then be expressed as

$$\lambda_3 = \frac{1}{\lambda_1\lambda_2} \tag{4.42}$$

Inserting (4.42) into (4.38) yields

$$\begin{cases} I_1 = \lambda_1^2 + \lambda_2^2 + \dfrac{1}{\lambda_1^2\lambda_2^2} \\ I_2 = \lambda_1^2\lambda_2^2 + \dfrac{1}{\lambda_2^2} + \dfrac{1}{\lambda_1^2} \end{cases} \tag{4.43}$$

The strain energy function $W(\lambda)$ has to fulfil some general conditions:

- $W(1) = 0$ for $\lambda = 1$, i.e. the strain energy is zero in the unloaded case.
- $W(\lambda) \to \infty$ for $\lambda \to 0$ and for $\lambda \to \infty$, i.e. the strain energy should increase for increasing compression and tension.
- $\dfrac{\partial W}{\partial \lambda} = 0$ for $\lambda = 1$, the nominal stress has to be zero in the unloaded state.

4.2.4 Polynomial form

A common strain energy function used in FE-programs describing the hyperelastic material is the polynomial form. This polynomial form contains the elastic constants in a linear dependence and is expressed in terms of invariants and yields

$$W = \sum_{i=0,\, j=0}^{\infty} C_{ij} (I_1 - 3)^i (I_2 - 3)^j \tag{4.44}$$

where C_{ij} are material parameters. The sum is normally just including a few terms and not written to infinity. As mentioned earlier, the strain energy density function has to fulfil some specific conditions. This is the reason for writing the series in terms of $(I_1 - 3)$ and $(I_2 - 3)$, as it gives $W = 0$ in the un-deformed state, if $C_{00} = 0$.

Using index sum less or equal to three, equation (4.45) can be written as

$$\begin{aligned} W = {} & C_{10}(I_1 - 3) + C_{01}(I_2 - 3) \\ & + C_{20}(I_1 - 3)^2 + C_{11}(I_1 - 3)(I_2 - 3) + C_{02}(I_2 - 3)^2 \\ & + C_{30}(I_1 - 3)^3 + C_{21}(I_1 - 3)^2 (I_2 - 3) + C_{12}(I_1 - 3)(I_2 - 3)^2 + C_{03}(I_2 - 3)^3 \\ & + \ldots\ldots \end{aligned} \tag{4.45}$$

The *neo-Hooke* strain energy function can be obtained from the polynomial form by only considering the first term, which yields,

$$W = C_{10}(I_1 - 3). \tag{4.46}$$

By experimental tests in compression and moderate shear, this neo-Hooke model has shown very good agreement. The conclusion can therefore be made that the first parameter, C_{10} is the most important parameter in the polynomial form.

By excluding terms that contains the second invariant, *Yeoh* found a model that gave a good fit to experimental tests for carbon-black-filled rubbers. With the parameter I_2 excluded in (4.45) he obtained the following strain energy function, called the Yeoh-model,

$$W = C_{10}(I_1 - 3) + C_{20}(I_1 - 3)^2 + C_{30}(I_1 - 3)^3 \tag{4.47}$$

The advantage of this model is that it is quite simple and the parameters can be found by only doing a shear test. This is not possible for general choice of parameters. Typical tension-compression and shear curves for a hyperelastic material according to Yeoh are illustrated in Figure 4.5.

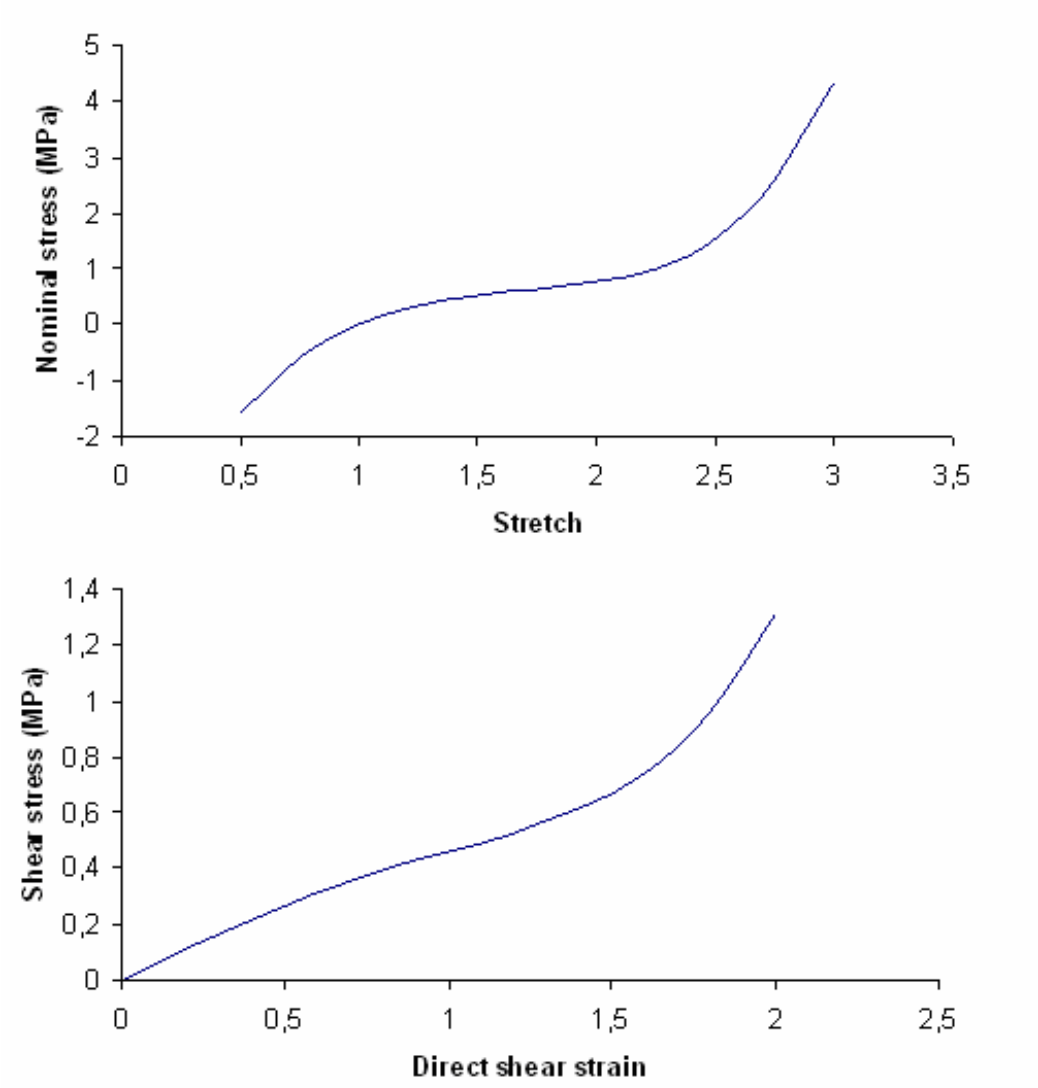

Figure 4.5: *Typical one-dimensional curves for a Yeoh-model exposed to tension-compression and shear.*

The described polynomial form is used in ANSYS but looks a little different. In ANSYS, the material is not assumed to be fully incompressible, and therefore consideration of volume changes is assumed, leading to changes of the strain energy function.

Definition of the volume-preserving part of the deformation gradient, $\overline{F}_{ij}$ is

$$\overline{F}_{ij} = J^{-1/3} F_{ij} \tag{4.48}$$

and thus

$$\overline{J} = \det\left[\overline{F}_{ij}\right] = 1 \tag{4.49}$$

The modified principle stretch ratios are then

$$\overline{\lambda}_p = J^{-1/3} \lambda_p \qquad (p = 1, 2, 3) \tag{4.50}$$

The strain energy potential can now be defined as

$$W = W(\bar{I}_1, \bar{I}_2, J) = W(\bar{\lambda}_1, \bar{\lambda}_2, \bar{\lambda}_3, J) \tag{4.51}$$

The polynomial form of the strain energy function in ANSYS takes the form,

$$W = \sum_{i,j=1}^{N} C_{ij} (\bar{I}_1 - 3)^i (\bar{I}_2 - 3)^j + \sum_{k=1}^{N} \frac{1}{d_k} (J-1)^{2k} \tag{4.52}$$

where N, C_{ij}, d_k are material parameters.

This polynomial form is dependent on the volumetric changes in the material. If the material is fully incompressible, the polynomial form will look like (4.44). No limitation is made on N in the ANSYS program. A higher N may provide a better fit to the exact solution; however, it may on the other hand cause numerical difficulties in fitting the material parameters.

The Yeoh model used in ANSYS is a reduced polynomial form and looks like

$$W = \sum_{i=1}^{N} C_{i0} (\bar{I}_1 - 3)^i + \sum_{k=1}^{N} \frac{1}{d_k} (J-1)^{2k} \tag{4.53}$$

With N = 3, used in this project, the Yeoh model yields

$$\begin{aligned} W = {} & C_{10}(\bar{I}_1 - 3)^1 + C_{20}(\bar{I}_1 - 3)^2 + C_{30}(\bar{I}_1 - 3)^3 \\ & + \frac{1}{d_1}(J-1)^2 + \frac{1}{d_2}(J-1)^4 + \frac{1}{d_3}(J-1)^6 \end{aligned} \tag{4.54}$$

The Yeoh-parameters used in this project came from a test made by Per-Erik Austrell and Erik Serrano at Lund University, Division of Structural Mechanics 2003. After discussion with Erik Serrano about how the test was carried out, the conclusion was that the material had been exposed to some stress softening, i.e. Mullins effect is in some way included in the parameters. The test specimens used in this project have not been conditioned in any way, which must be kept in mind when experimental tests are compared to the FE-simulations.
The experimental test for finding the proper Yeoh-parameters can be found in Appendix A.

4.3 The finite element method

In this section an introduction to the finite element method will be carried out, as well as the implementation for which the updated Lagrangian method is used.

4.3.1 Introduction to the finite element method

Here the text is based on the literature *Introduction to the Finite Element Method* written by Niels Saabye Ottosen and Hans Petersson [8].

Many problems encountered in engineering mechanics are too complicated to solve with classic analytical methods. These are instead modelled by differential equations and solved in an approximate manner. The numerical method by which the differential equations are solved is called *Finite Element Method*. The body to be analysed is divided into smaller parts, so-called finite elements, so that an approximation can be made for each of these parts instead of seeking an approximation that holds for the entire body. This approximation has many advantages. For instance, even though the variable varies in a highly non-linear manner over the entire body, it may be a fair approximation to assume that the variable varies in a linear fashion over each element. The collection of all elements is called a *finite element mesh*.

When the approximate behaviour of all the elements have been determined, these elements are patched together in order to obtain a solution for the behaviour of the entire body.

The approximation for the different elements is usually a polynomial that control variable changes over each of these elements. In mechanical problems, this variable is often the displacement. It is assumed that the variables are known at certain points, called nodal points and are in most cases located at the boundary of each element. The elements are also connected to each other at these nodal points. Each node has a number of degrees of freedom (DOF). In a mechanical problem with solid elements, the DOF:s represent the displacement in three directions (x, y, z) and sometimes also rotation in three directions (R_x, R_y, R_z). It is the specific approximation that controls how the variable changes over each element.

In general a complete FE-simulation consists of the following steps:

- Create or import the geometry of the model.
- Choose a material model and assign material properties to the different parts of the model.
- Create an appropriate mesh for the model.
- Define parts that may come into contact with each other.
- Define loads and boundary conditions.
- Create steps in which it is defined how and under what duration the loads and boundary conditions apply.
- Perform analysis.
- Study and evaluate the results.

4.3.2 Finite element implementation

The text in this section is based on [6] and will here only give the essential equations. For a more elaborate description, the reader is referred to [6].

The finite element implementation for the updated Lagrangian formulation must consist of the current geometry with current volumes and surfaces. The virtual strain increments refer to the current geometry and the stresses are the Cauchy stresses as described earlier in this chapter. The virtual work equation (4.7) is here expressed in matrix form as

$$\int_V \delta\varepsilon\, \sigma\, dV = \int_S \delta\mathbf{u}\, \mathbf{t}\, dS + \int_V \delta\mathbf{u}\, \mathbf{b}\, dV \tag{4.55}$$

Where the left hand side is the incremental internal work and the right hand side is the incremental external work.

The virtual and incremental displacements $\delta\mathbf{u}(\mathbf{x})$ and $d\mathbf{u}(\mathbf{x})$ are considered as functions of the current configuration $\mathbf{x}$. This implies a representation of the virtual displacement in the form

$$\delta\mathbf{u}(\mathbf{x}) = \sum_n h_n(\mathbf{x})\delta\mathbf{u}_n \tag{4.56}$$

in terms of shape functions $h_n(\mathbf{x})$ and nodal values $\delta\mathbf{u}_n$, $n = 1, 2, \ldots$. The same expression holds for the nodal values $d\mathbf{u}_n$.

To define the equivalent external nodal forces $\mathbf{f}_n^{ext}$, the right hand side of the virtual work equation (4.55) is used via the relation

$$\delta V_{ext} = \delta\mathbf{u}_n^T \mathbf{f}_n^{ext} = \delta\mathbf{u}_n^T \left\{ \int_S h_n(\mathbf{x})\, \mathbf{t}\, dS + \int_V h_n(\mathbf{x})\, \mathbf{b}\, dV \right\} \tag{4.57}$$

where summation over the nodes n = 1, 2, … is implied, and loads refer to current surfaces and volumes. This gives the external nodal forces as

$$\mathbf{f}_n^{ext} = \int_S h_n(\mathbf{x})\, \mathbf{t}\, dS + \int_V h_n(\mathbf{x})\, \mathbf{b}\, dV \tag{4.58}$$

As can be seen from this equation, the external nodal forces are traction- and body forces are weighted by the corresponding shape function $h_n(\mathbf{x})$ and integrated over the current surface and volume.

The internal nodal forces are defined in the same manner as the external nodal forces, i.e. by use of the virtual work. Here the internal virtual work is used and the expression yields

$$\delta V_{\text{int}} = \delta\mathbf{u}_n^T \mathbf{f}_n^{\text{int}} = \delta\mathbf{u}_n^T \left\{ \int_V \mathbf{B}_n(\mathbf{x})^T\, \sigma\, dV \right\} \tag{4.59}$$

This scalar work equation generates the internal nodal forces

$$\mathbf{f}_n^{\text{int}} = \int_V \mathbf{B}_n(\mathbf{x})^T\, \sigma\, dV \tag{4.60}$$

where the strain interpolation matrix $\mathbf{B}_n(\mathbf{x})$ is a function of the derivatives of the shape functions. The calculation of the internal nodal forces requires evaluation of a volume integral of the product of the current Cauchy stress and the strain representation matrix $\mathbf{B}_n(\mathbf{x})$.

For the forces to be in equilibrium, the external forces, $\mathbf{f}_n^{ext}$ should be equal to the internal forces, $\mathbf{f}_n^{\text{int}}$. As the problem at hand is non-linear, a solution technique for finding the equilibrium must be introduced. Therefore the next section will describe the *Newton-Raphson method* which is used in this project.

4.4 The Newton-Raphson method

In the problem, equilibrium or deviation from equilibrium is expressed in terms of the nodal residual forces

$$\mathbf{R}_n = \mathbf{f}_n^{ext} - \mathbf{f}_n^{\text{int}} \tag{4.61}$$

This residual is by an iterative procedure eliminated using the linearization of $\mathbf{R}_n$,

$$d\mathbf{R}_n = \frac{d\mathbf{R}_n}{d\mathbf{u}_m} d\mathbf{u}_m \tag{4.62}$$

Where the first term of the right hand side is the tangent stiffness matrix and from the incremental virtual work the stiffness matrix is obtained,

$$d(\delta V_{\text{int}}) = \delta\mathbf{u}_n^T \mathbf{K}_{nm} d\mathbf{u}_m = \delta\mathbf{u}_n^T \left\{ \mathbf{I} \cdot \int_V \frac{\partial h_n}{\partial x_\alpha} \sigma_{\alpha\beta} \frac{\partial h_m}{\partial x_\beta} dV + \int_V \mathbf{B}_n^T \mathbf{C} \mathbf{B}_m dV \right\} d\mathbf{u}_m \tag{4.63}$$

The tangent stiffness is thereby defined as

$$\mathbf{K}_{nm} = \mathbf{I} \cdot \int_V \frac{\partial h_n}{\partial x_\alpha} \sigma_{\alpha\beta} \frac{\partial h_m}{\partial x_\beta} dV + \int_V \mathbf{B}_n^T \mathbf{C} \mathbf{B}_m dV \tag{4.64}$$

Where **I** is the two dimensional unit tensor, and **C** is the linearization of the stress tensor for the updated Lagrangian method. This constitutive tensor can with the use of (4.23) and (4.27) be connected to the constitutive tensor, $C^0_{\alpha\beta\gamma\delta}$ given by the original configuration. In index notation the expression yields

$$C_{\xi\eta\kappa\lambda} = \frac{\partial x_\xi}{\partial x^0_\alpha} \frac{\partial x_\eta}{\partial x^0_\beta} \frac{C^0_{\alpha\beta\gamma\delta}}{J} \frac{\partial x_\kappa}{\partial x^0_\gamma} \frac{\partial x_\lambda}{\partial x^0_\delta} \qquad \text{where} \qquad C^0_{\alpha\beta\gamma\delta} = 4\frac{\partial^2 W}{\partial C_{\alpha\beta} \partial C_{\gamma\delta}} \tag{4.65}$$

Where the two first- and last terms in the left equation are the deformation tensor given by equation (4.4).

To solve the problem at hand, the mentioned Newton-Raphson method will be used. In its standard form it consists of a series of prescribed load increments combined with an iterative solution of the equilibrium equations for the corresponding displacement increments.

The iterative process for one incremental load step, by an increase of the external force $\mathbf{f}_n^{ext}$, in its general form will here be presented.

1. The system is in an equilibrium state

2. From the equation

$$K_i^T \Delta u_i = f^{ext} - f_i^{\text{int}}, \tag{4.66}$$

the incremental displacement Δu_i is calculated. In the first iteration for each load step the stiffness matrix K_i^T and the internal force f_i^{int} are calculated from the earlier equilibrium state. For other iterations these are updated to yield for the current state.

3. With Δu_i the deformation for the current state is defined as,

$$u_{i+1} = u_i + \Delta u_i . \tag{4.67}$$

In this new current state the internal force f_i^{int} can be calculated.

4. Step 2 and 3 are repeated until the equilibrium is obtained, i.e. $f^{ext} \approx f_i^{\text{int}}$. This iterative process is shown in Figure 4.6.

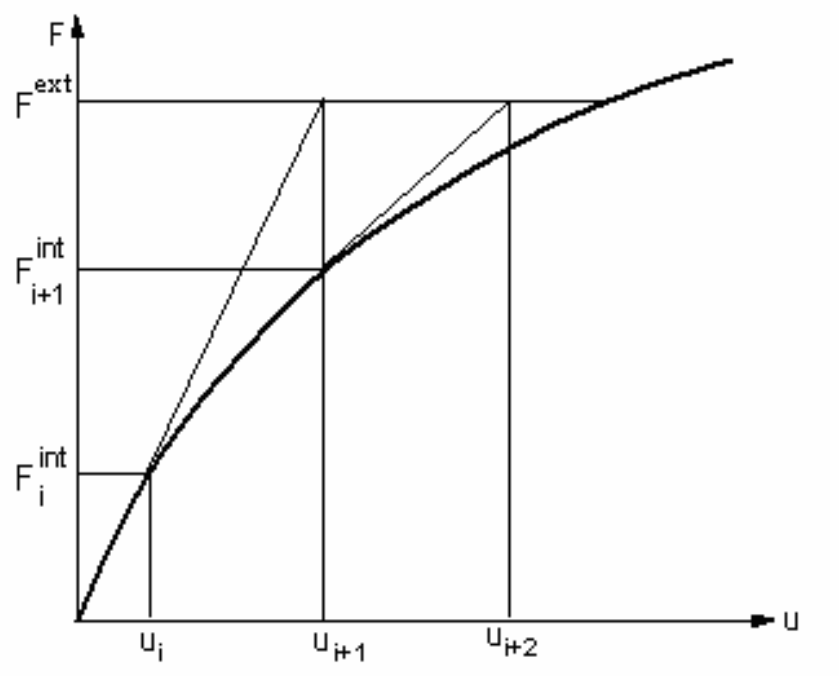

Figure 4.6: *Newton-Raphson iteration*. [2]

For non-linear problems ANSYS uses as default the *full Newton-Raphson method*, meaning that the tangent stiffness matrix is updated for each new iteration step. There is also a possibility to use the so-called *modified Newton-Raphson method*, which calculates the stiffness matrix less frequently. This could be efficient for large system when it is a great computational cost to re-calculate the tangent stiffness matrix, but the convergence could be a problem for this modified method.

4.4.1 Convergence

The purpose of the Newton-Raphson method is to achieve a state of equilibrium for every load step. This is made by an iterative process that continues until a certain convergence criteria have been fulfilled, which is based on the residual given in equation (4.61). Convergence is assumed when,

$$\left\|\mathbf{R}\right\| < \varepsilon \cdot R_{ref} \tag{4.68}$$

where ε is a tolerance and R_{ref} is a reference value. The norm of **R** used in this specific problem is set to

$$\left\|\mathbf{R}\right\| = (\sum R_i^2)^{\frac{1}{2}} \tag{4.69}$$

which is the square root of the sum of the squares value of the terms.

The used convergence tolerance in this project is the default value in ANSYS, which is set to 0.001.

4.4.2 Line search

To solve a problem with a non-linear character, the problem is divided into small linearized sub steps. For the kind of problems that includes several variables it is important that the step is not too large. To optimize the length of this step a technique called *line search* is used. This technique evaluates the magnitude of the step in the direction defined by each linearized sub step. The advantage of the line search is that an improved approximation is obtained by only solving a one dimensional problem. Even for a rather crude line search a substantial improvement can be made. For problems involving contact, ANSYS automatically uses the line search function.

Consider equation (4.67)

$$u_{i+1} = u_i + \Delta u_i \tag{4.70}$$

The use of the full Δu_i can sometime gives instability in the solution process. By using the line search, equation (4.70) becomes,

$$u_{i+1} = u_i + s \cdot \Delta u_i \tag{4.71}$$

where *s* is the line search parameter, 0.05 < s < 1.

Finding a proper value of *s* is made by minimizing the energy of the system, considered by the following equation,

$$g_s = \Delta u_i^T \cdot (F^{ext} - F^{\text{int}}(s \cdot \Delta u_i)) \tag{4.72}$$

where g_s = gradient of the potential energy with respect to *s*.

An iterative solution is used to solve equation (4.72). In ANSYS, iterations are continued until either,

1. g_s is less than $0.5 \cdot g_0$, where g_0 is the value of equation (4.72) at $s = 0.0$.
2. g_s is not changing significantly between iterations.
3. Six iterations have been performed.

If $g_0 > 0.0$, no iterations are being performed and *s* is set to 1. *s* is not allowed to be lower than 0.05.

Table 4.1 shows the iterative scheme for the Newton-Raphson method with line search.

---

load steps $n = 1, 2, \ldots$

$\mathbf{f}_n^{ext} = \mathbf{f}_{n-1}^{ext} + \Delta\mathbf{f}_n^{ext}$

$\mathbf{u}_n^0 = \mathbf{u}_{n-1}$

iterations $i = 1, 2, \ldots$

$\mathbf{K}_n^{i-1} = \dfrac{d\mathbf{f}^{\text{int}}(\mathbf{u}_n^{i-1})}{d\mathbf{u}}$

$\mathbf{R}_n^i = \mathbf{f}_n^{ext} - \mathbf{f}^{\text{int}}(\mathbf{u}_n^{i-1})$

$\Delta\mathbf{u}_n^i = (\mathbf{K}_n^{i-1})^{-1}\mathbf{R}_n^i$

$R_0 = (\Delta\mathbf{u}_n^i)^T \mathbf{R}_n^i$

$s_0 = 0 \ , \ s_1 = 1$

line search iterations $k = 1, 2, \ldots$

$\mathbf{u}_n^i = \mathbf{u}_n^{i-1} + s_k \Delta\mathbf{u}_n^i$

$\mathbf{R}_n^i = \mathbf{f}_n^{ext} - \mathbf{f}^{\text{int}}(\mathbf{u}_n^i)$

$R_k = (\Delta\mathbf{u}_n^i)^T \mathbf{R}_n^i$

line search convergence

stop iterations i when $\left\| \mathbf{R}_n^i \right\| < \varepsilon \left\| \mathbf{R}_{ref} \right\|$

end of load step n

Table 4.1: *The Newton-Raphson method with line search.* [6]

Chapter 5

Experiments

The main purpose of the experimental tests was to create force-deformation curves for a gasket exposed to compression. The force-deformation curves should represent the compression of the gasket until the plates nearly reach metallic contact. These tests were performed for both geometries and material types. The gasket was compressed by a horizontally rigid plate, as it reflects the reality in the best possible way. If the gasket had been compressed by a corrugated plate the force would act on the plate and not the gasket. To avoid this, a horizontal rigid plate was therefore used instead. The ultimate scenario would have been to compress the gasket by a corrugated plate with a gasket on top to centre the force to the lower gasket. This model could not fit into the test equipment on Alfa Laval and would have required a lot of computational effort in ANSYS.

This chapter describes how the tests were performed, their result, and their sources of error. At first, tests were only to be made on the test equipment provided by Alfa Laval. As will be seen in the results, the uncertainty and the sources of error on the equipment made it necessary to perform further testing at LTH.

5.1 Tests at Alfa Laval

5.1.1 Objective

This test had two purposes, where the primary was to create force-deformation curves. As the test equipment has the primary purpose of being a calibrating tool, an evaluation of the test equipment in aspect of its usefulness for our kind of test was performed.

5.1.2 Equipment

The test was made with equipment from Alfa Laval; see Figure 5.1. The equipment includes two parts; a compression device and a box with a force display. Between the two identical blocks in the compression device, the plate and gasket are placed; see Figure 5.2. The bottom block is fixed while the upper block moves down when the screw thread cylinder is pressing at it. There is a load cell in the bottom block for registration of the gasket force.

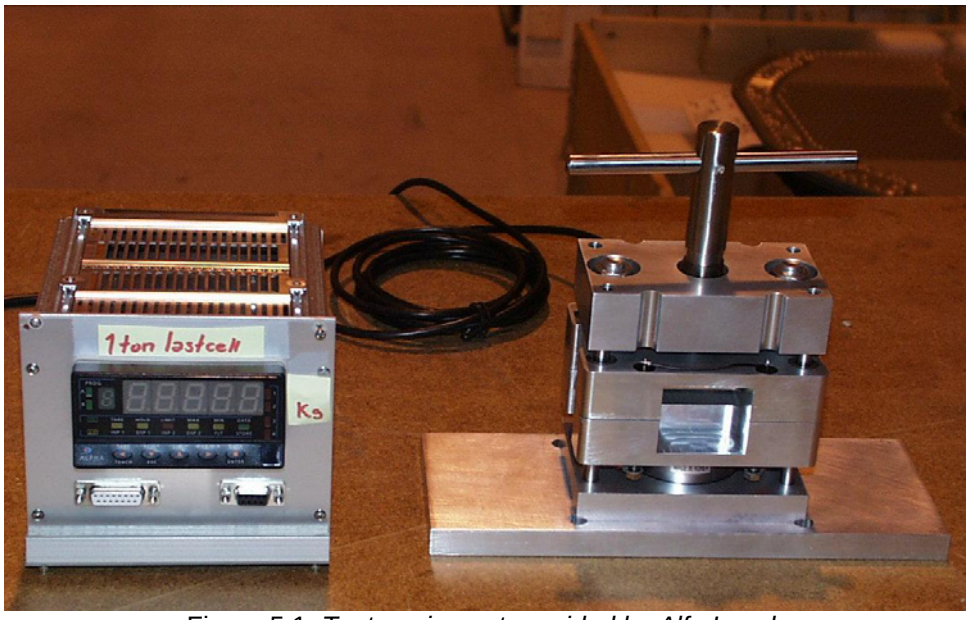

Figure 5.1: *Test equipment provided by Alfa Laval.*

Figure 5.2: *Compression device with the plate and gasket inserted.*

The test specimen of the plate was a cut out piece from a complete plate. The gasket specimen for the test was taken from a complete gasket and cut up with the same length as the plate, although there were differences in length between the different specimens. This difference depended on the cutting process, which did not allow a better accuracy. The tolerance was approximately ± 1 mm. The plate was fixated on an aluminium metal block, with a double-sided tape; see Figure 5.3, in order to have the same plate position for every test.

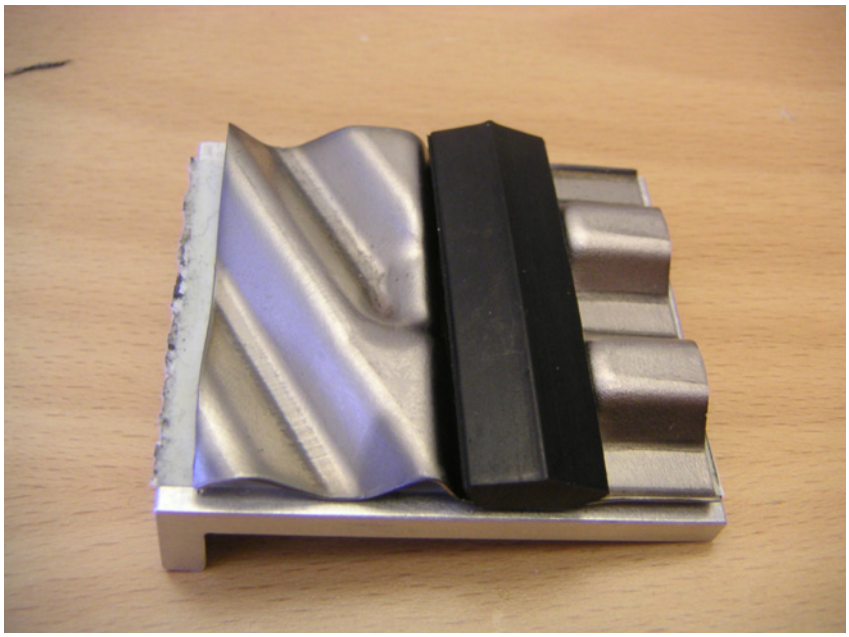

Figure 5.3: *Plate and gasket. The plate is fixated with tape to an aluminium plate.*

5.1.3 Implementation

The deformation of the gasket was measured as the difference in distance between the two blocks in the un-deformed- and the current state. The distance was measured with the use of feeler gauges. During the deformation process the upper block became horizontally unbalanced which caused problems when to measure the deformation. Due to this problem, the deformation of the gasket became irregular, which gave problem in defining the correct deformation. The deformation process was therefore ended when the first corner reached the desired position, in order to be sure that no metallic contact appeared between the plate and the upper block, as that would not only measure the pure gasket force but also the force needed to deform the plate.

For each quarter of a revolution with the screw thread cylinder, the force and deformation was measured. As the block was unbalanced during the deformation, a mean value of the four corners displacements was carried out as the deformation of the gasket. The force was registered after the measurement of the displacements, which gave a converged value of the force, with respect to the relaxation in the gasket. The time for relaxation was approximately two minutes, and with a low speed of deformation, this was considered to be nearly the converged value of the relaxation.

To avoid viscous effects, the velocity of deformation was low, approximately three minutes for a quarter of a revolution (1/4 mm compression of the gasket). When the end point had been reached, the deformation was kept under a period of 15 minutes, for finding the converged value of the relaxed force. With all force- and deformation data points, a force-displacement curve was created.

Before the tests were carried out, it was recognized that the velocity of deformation influenced the relaxed force in the gasket. As a result of this, four tests were decided to be carried out. This was done with two slow speed- and two fast speed tests. The deformation was measured as 1.75 revolutions of the screw thread cylinder. The tests with the slow velocity of deformation were carried out with the same speed as the other tests. The high-speed tests were carried out with a significant higher velocity of deformation.

5.1.4 Results

Here the results for the tests at Alfa Laval are presented. It will start out with the tests for geometry 1, with NBR as gasket material and thereafter for geometry 2, with both NBR and EPDM. The test for checking if the relaxed force is rate dependent will also be presented in the ending of this section.

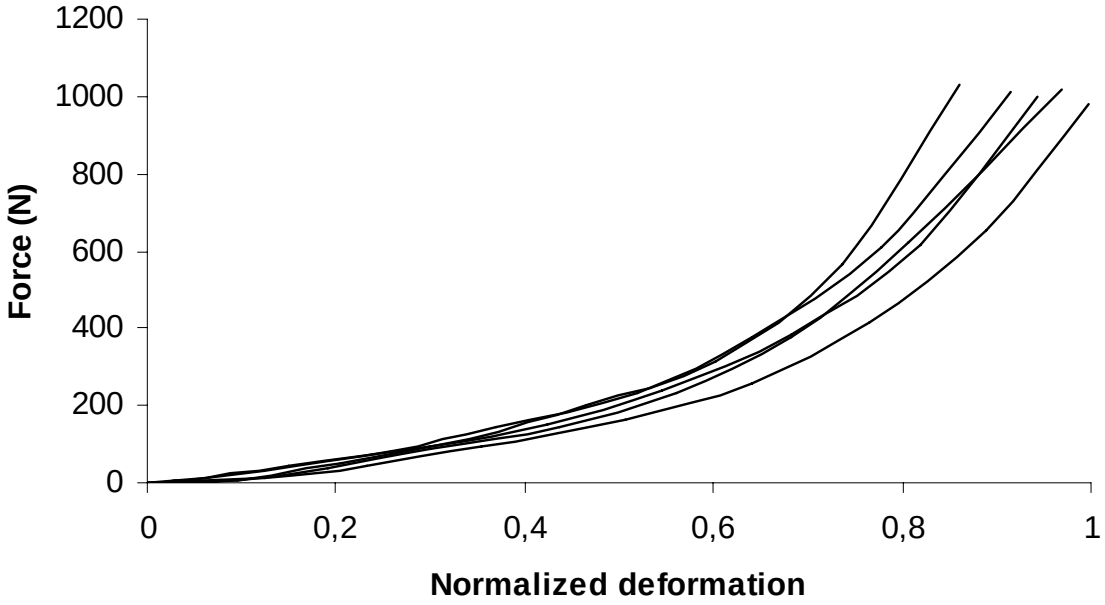

Figure 5.4: *Five force-deformation curves for geometry 1 with NBR*.

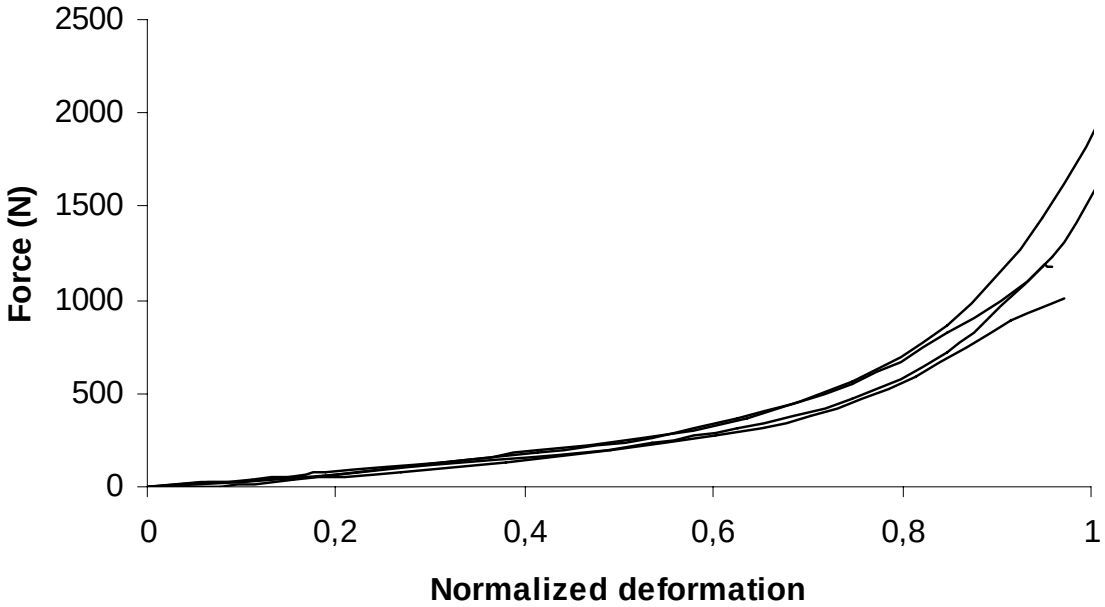

Figure 5.5: *Four force-displacement curves for geometry 2 with NBR*.

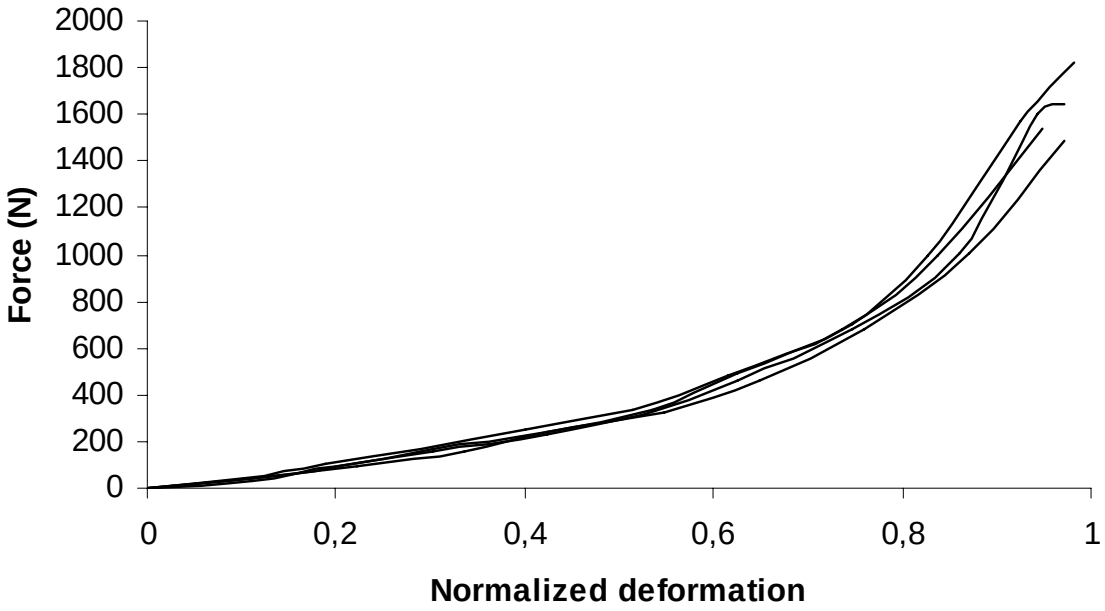

Figure 5.6: *Four force-displacement curves for geometry 2 with EPDM*.

1,75 revolution	max force (N)	relaxed force (N)	time of relaxation (h)
Test 1 (slow)	1016.3	845.6	3.3
Test 2 (slow)	977.1	795.6	3.8
Test 3 (fast)	1958.1	1346.9	24.0
Test 4 (fast)	2423.1	1622.6	24.0

Table 5.1: *Rate dependence test*

Commentary

Geometry 1, NBR, shows significant differences between the tests. As for geometry 2, the difference is not so obvious but still quite large. As the upper block gets horizontally unbalanced during the deformation and as it is measured as a mean value, the total deformation differs between the tests and there cannot be any certainty of how the gasket have been deformed.

For geometry 2, the results are improved in aspects of similarity between the tests. These tests were carried out after geometry 1 and maybe a better routine for implementing the tests had been developed, and therefore the tests show a better accuracy.

With the uncertainty of the results, tests were decided to be carried out at LTH. The purpose of these tests were to have excess to a better test equipment, in aspect of a more stabile deformation process and more accurate measuring equipment, and therefore to achieve more reliable results.

As mentioned earlier there was a significant difference in the relaxed forces depending on the velocity of deformation. From Table 5.1 one can see that the maximum force is 1000-1500 N larger for the high speed tests. Although the time of relaxation is around seven times higher

for the high-speed tests, they do not seem to converge to the same value as the low speed tests. As there is no logical explanation of this phenomenon, test was carried out at LTH for further investigation.

As a result of the earlier discussion, the test equipment must be improved to be able to produce an accurate and reliable result. A more stable horizontal block should be developed and also a better way to measure the deformation. There is also an uncertainty of using feeler gauge. Until the test equipment has been improved, it should not be used for these kinds of tests.

5.1.5 Sources of error

There are two main sources of error with the test equipment at Alfa Laval. The first is the earlier described problem with the upper block. How to handle this is not fully investigated. A check at the results shows that the relaxed forces are almost the same but the mean values of the deformation vary. As the upper block is horizontally unbalanced the deformation of the gasket could not be perfectly measured and therefore the best approximation is to choose a mean value of the four corners.

Measurement of the displacement by use of feeler gauges also gave problems when defining the initial distance between the blocks. It is a risk that the feeler gauge pushes the upper block to a new starting position, resulting in less total compression of the gasket. When the distance between the two blocks is greater than two millimetres, the use of two combined feeler gauges is necessary. As there may be a small gap between the gauges, the measured thickness can result in being smaller than it really is. This also affects the total deformation of the gasket.

A third source of error is the position of the gasket on the plate. The width of the gasket is smaller than the channel of the plate, where the gasket is placed. It is impossible to know if the gasket places itself in the middle, to the left or to the right of the plate channel, see Figure 5.7. The position of the gasket in the channel probably affects the force of compression, as the geometry of the plate differs from the left- and right side. The edges of the plate affect the possibility for the gasket to deform, and thereby affecting the force.

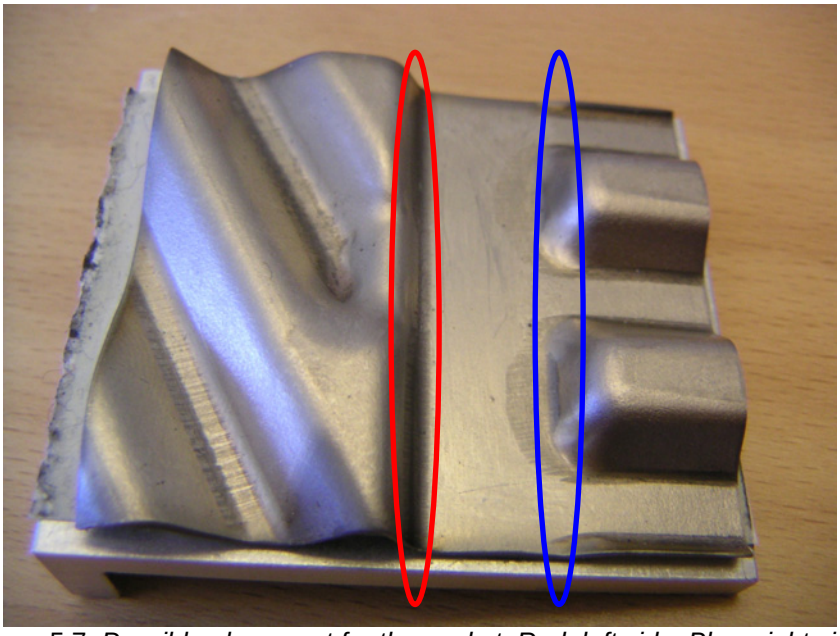

Figure 5.7: *Possible placement for the gasket. Red=left side, Blue=right side*.

5.2 Tests at LTH

5.2.1 Objective

The purpose of the tests at LTH was to get a controlled deformation in aspects of speed, and also to have access to better test equipment for measuring force and deformation. This equipment also ensures a reasonable horizontal deformation in comparison with the one supplied by Alfa Laval. During the test at Alfa Laval the velocity of deformation strongly affected the relaxed force. Tests were therefore performed with different velocity of deformation to investigate the phenomenon further. Tests were performed for both materials and geometries.

5.2.2 Equipment

The department of Solid Mechanics at LTH has in their laboratory a MTS (Material Test System) machine used for tension/compression experiments, Figure 5.8. This equipment was used for the testing at LTH. The machine includes a tension/compression unit, a control unit and a computer for gathering the data. The tension/compression part includes one fixed part and one movable part controlling the deformation by use of hydraulic. This equipment gives the possibility to carry out deformation-controlled tests.

Figure 5.8: *Test equipment at LTH*.

5.2.3 Implementation

The plate with the gasket was placed between the compression parts. An aluminium plate was placed on top of the gasket, Figure 5.9, in order to recreate the same scenario as the tests at Alfa Laval. During the tests, the movable part always started and ended at the same positions.

The gaskets were therefore not compressed in the same way for all tests, as there is a tolerance in height for the gaskets. From the test data it is possible to find the specific starting point when the gasket begins to deform.

The first thing investigated was the phenomenon with different relaxed forces depending on the velocity of deformation. Two different velocity of deformation was tested, 0.027 mm/s and 1.6 mm/s, i.e. 60 times faster.

The second part of the testing was to find data for the relaxed force-deformation curve for all test objects. To find the relaxed force values, the deformation was held constant at a number of specific positions during the test. The deformation was held for approximately 5 minutes. With a low velocity of deformation this pause was sufficient enough to get the converged value of the relaxed force. To create the force-deformation curve, the relaxed values of the force and their deformation were plotted.

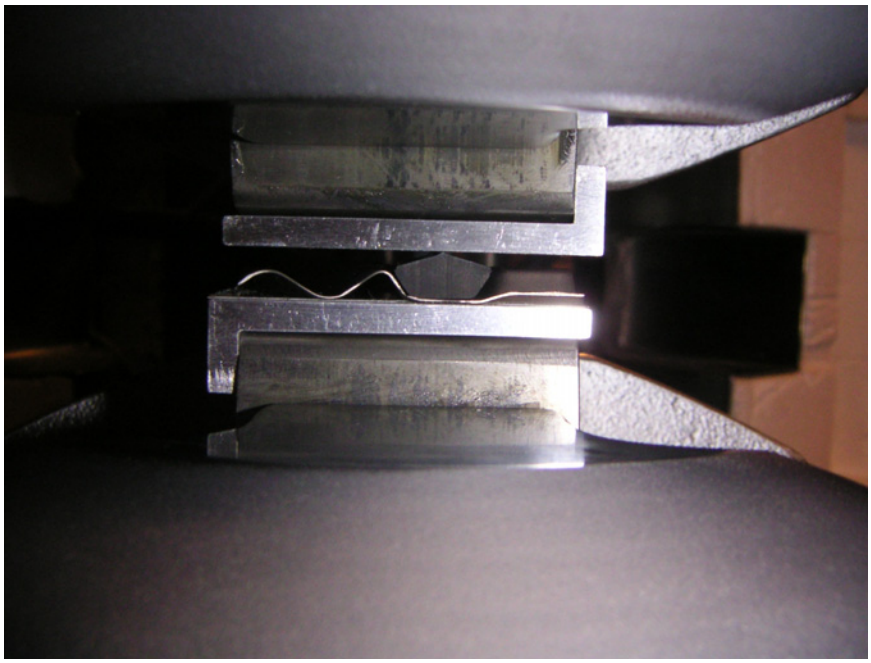

Figure 5.9: *Plate and gasket between the two compression parts*.

5.2.4 Results

In this section the results from the tests performed at LTH will presented. The first part is to see if there is any rate dependency that affects the relaxed forces. The second part will show the force-deformation curves for the different test objects.

5.2.4.1 Part 1

The gasket used for this investigation was geometry 1. The results will here be presented.

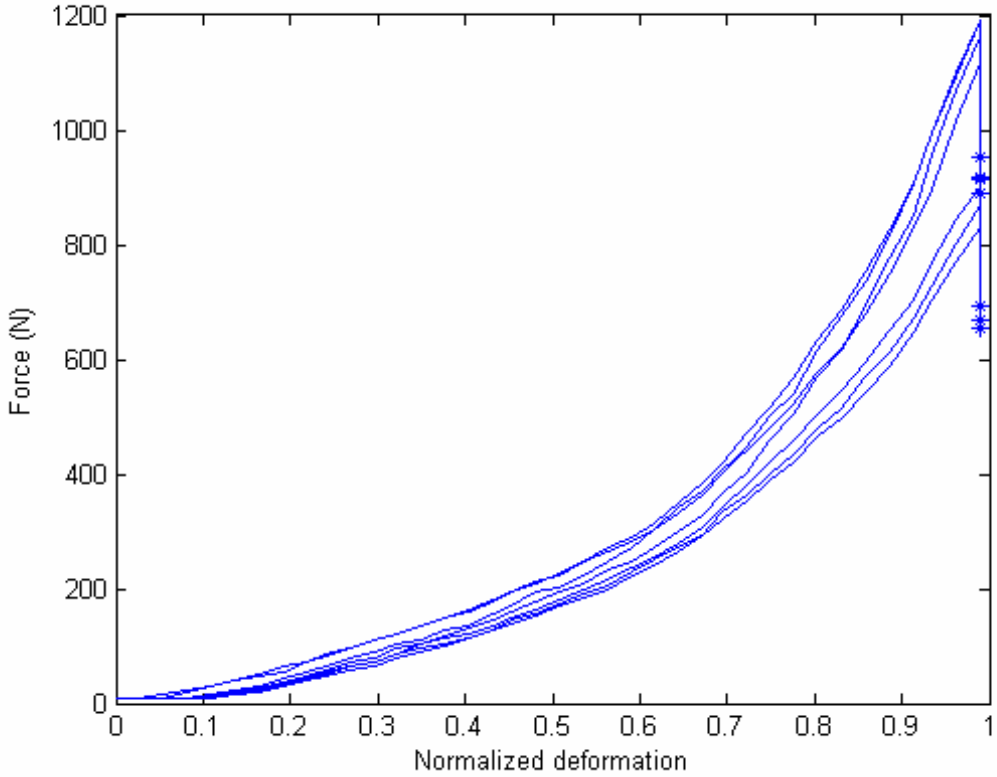

Figure 5.10: *Tests with a velocity of deformation of 0.027 mm/s, * = relaxed force at the total deformation*.

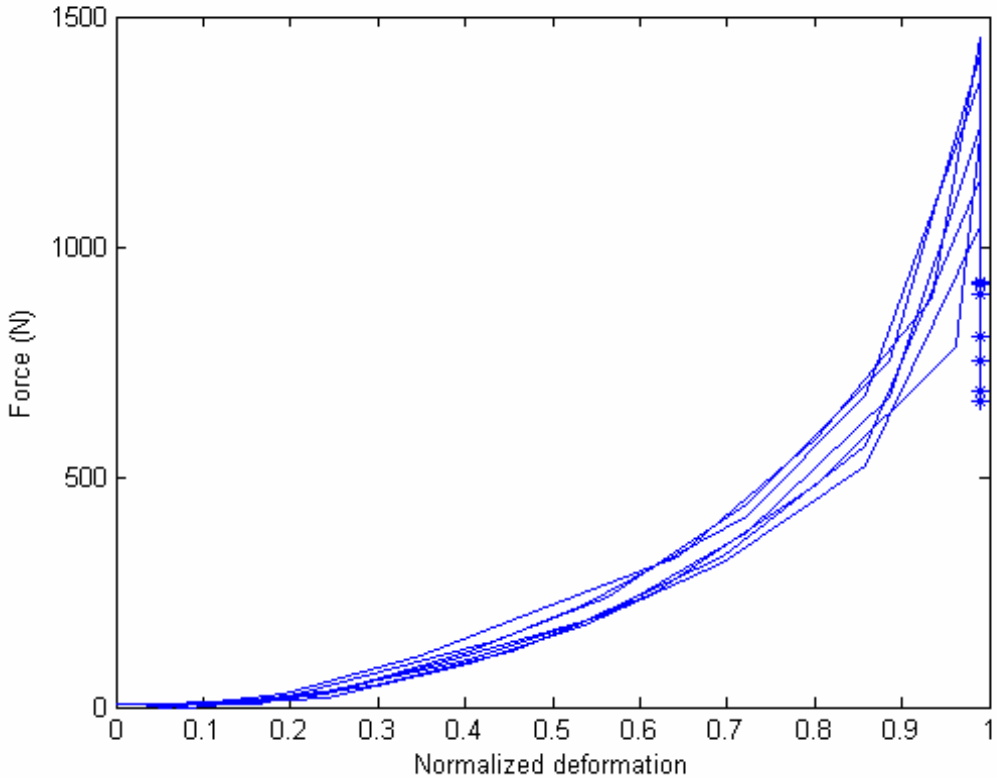

Figure 5.11: *Test with a velocity of deformation of 1.6 mm/s, *= relaxed force at the total deformation.*

Commentary

Even though the sampling frequency was set relatively high for the high-speed tests, the starting point for the deformation was too difficult to find. In the two plots, Figure 5.10 and 5.11, from the tests the actual starting point is therefore not considered, instead an assumption is done that the tests have the same spread in starting points. The relaxed force values for the tests are in the same range between 650-1000 N. Based on the results from this test, the conclusion is that the velocity of deformation does not affect the relaxed force value. Even for a much lower velocity of deformation, the relaxed force take the same value as the high-speed tests, which can be seen in Figure 5.12.

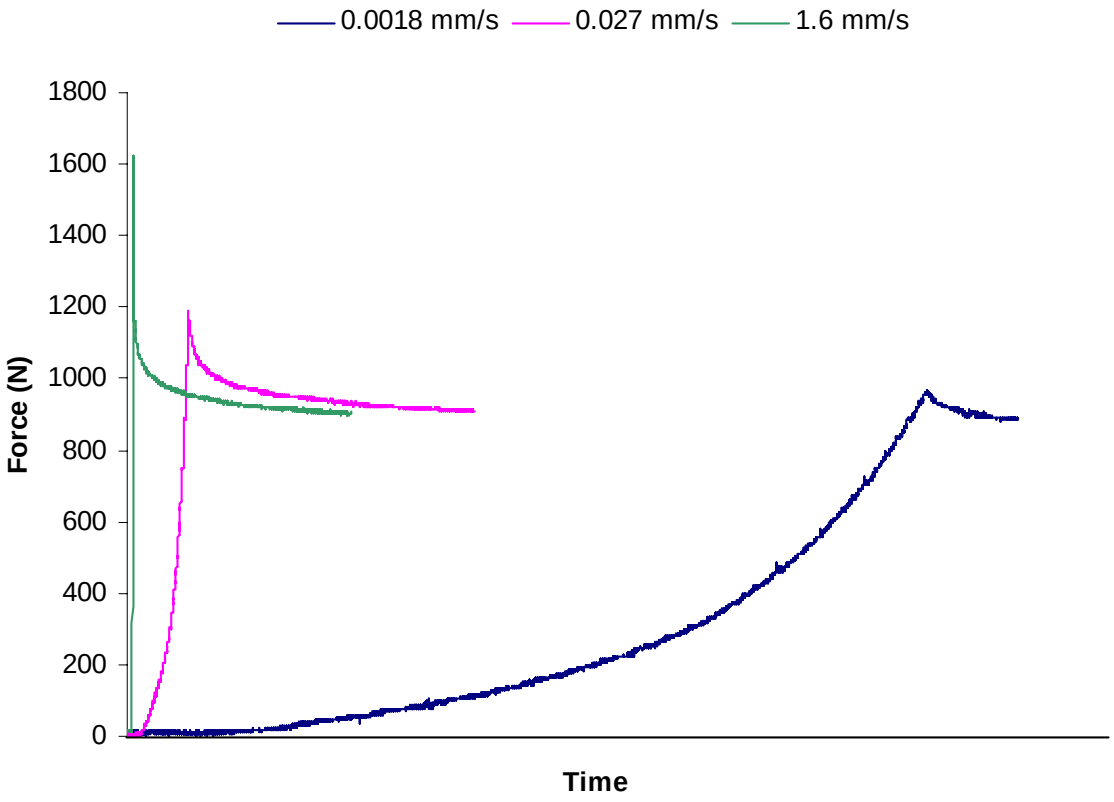

Figure 5.12: *Force-time curves for different speed of deformation.*

From Figure 5.12 the viscoelastic property for rubber is here obvious and one can se that the forces tend to converge to the same value. These effects are important to consider when the complete PHE is assembled. When the bolts are tightened at high speed, failure can occur.

With the same tests at Alfa Laval in mind, a further investigation with real test specimen and a more advanced way of measuring the total deformation is therefore desirable.

5.2.4.2 Part 2

For this part, three test specimens were used for each test, to create the force-deformation curves. The specimens were chosen with respect to their height. The purpose was to get test specimens with the same height in order to have the same deformation for all tests. The test procedure was performed by dividing the deformation into several sub steps, where the relaxed force was taken for each of these steps as can be seen in Figure 5.13.

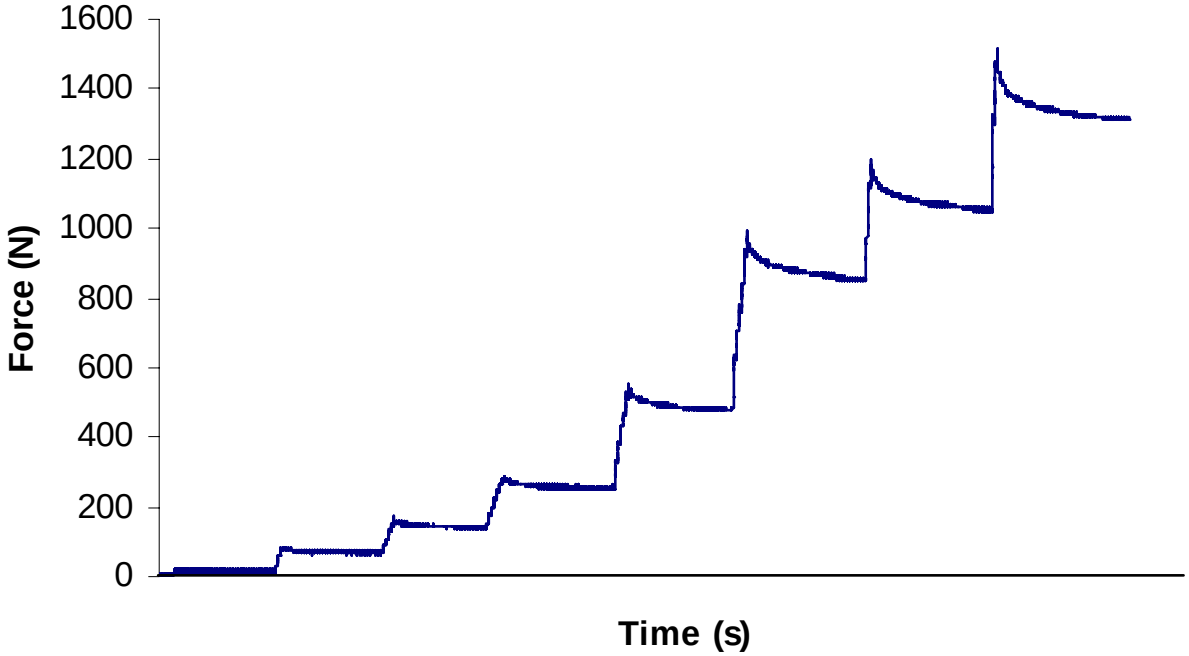

Figure 5.13: *A typical force-time curve for this test.*

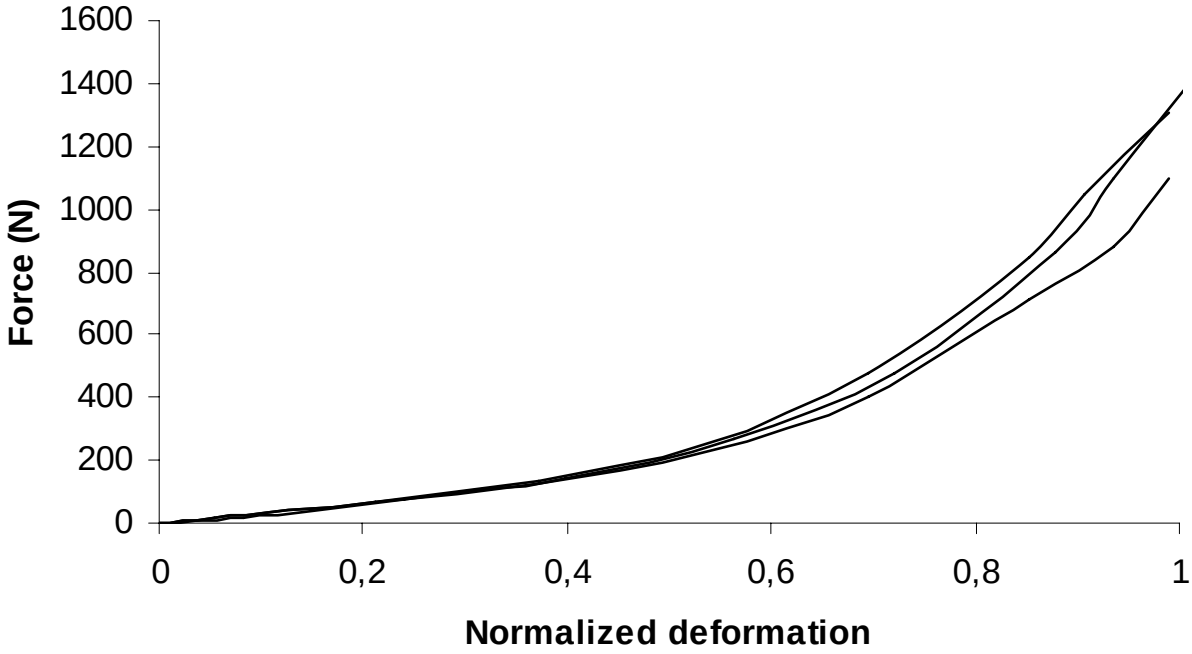

Figure 5.14: *Three force-deformation curves for geometry 1 with NBR*.

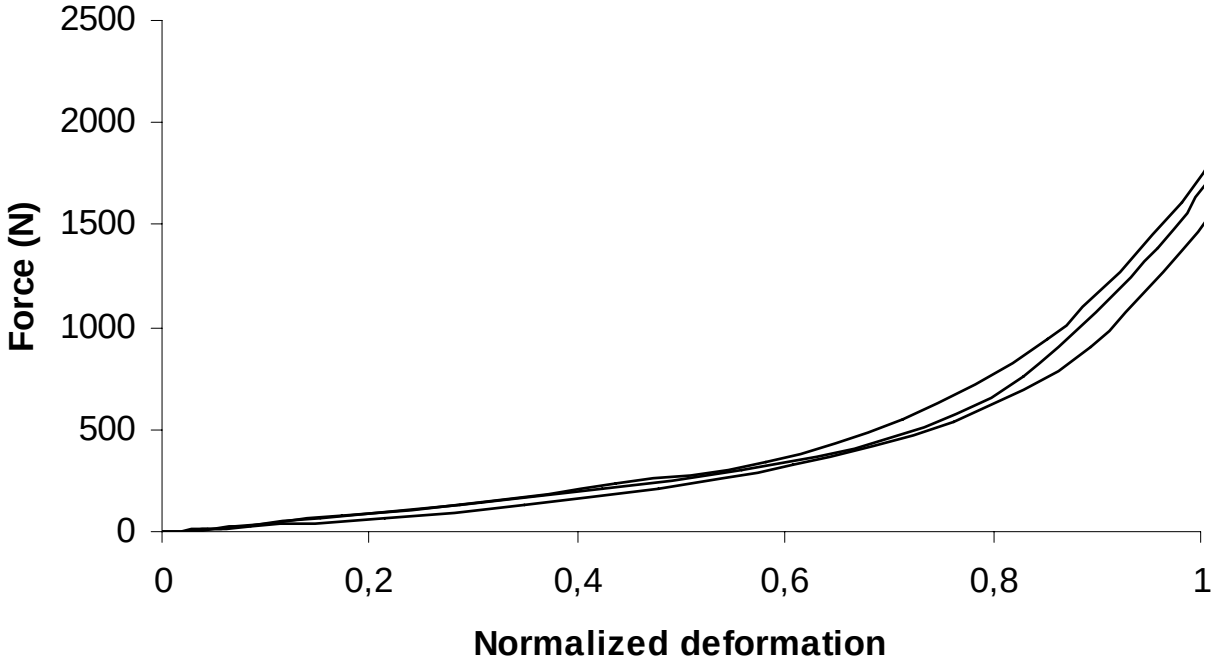

Figure 5.15: *Three force-deformation curves for geometry 2 with NBR*.

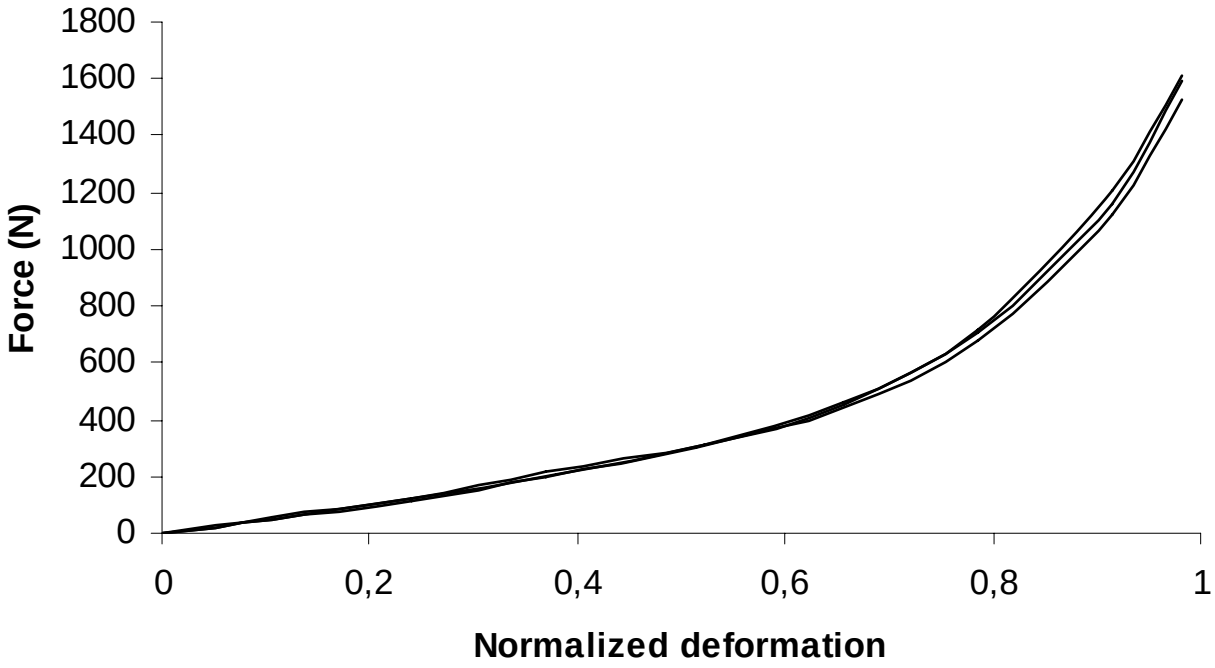

Figure 5.16: *Three force-deformation curves for geometry 2 with EPDM*.

Commentary

For the results from the tests at LTH, Geometry 1 with NBR has some spread results. For Geometry 2 with EPDM the tests are more equal to each other. Maybe more tests are required for all specimens, in order to get more reliable results. Although there are some differences between the tests, these tests are considered more reliable than the tests performed at Alfa Laval. Differences in test results are not unusual as several factors affect the result. Therefore differences in the results have to be expected.

5.2.5 Sources of error

As mentioned before with the errors for the test at Alfa Laval, this test also has the problem with the position of the gasket, see Figure 5.7. The other problem is to find the point when the deformation of the gasket begins. With a low sampling frequency, there is a possibility to miss important phases, such as the start of deformation of the gasket. With the high-speed test, the sampling frequency was set relatively high but the starting point was even though difficult to find.

Tolerance in the measuring equipment also complicated this problem. This is due to that the measuring is made in interval of 0.05 mm. For an example 0.08 mm is rounded off to 0.1 mm and 0.07 mm is rounded off to 0.05 mm. Therefore two tests measured to have the same deformation can actually have a difference of 0.05 mm.

Chapter 6

FE-model

In this chapter the FE-model is described. The model consists of a rubber gasket specimen surrounded by a corrugated plate and a plane horizontal plate. It is the vertical groove and the vertical gasket in the plate heat exchanger that constitutes the model in this project.

There is symmetry in the corrugated plate, see Figure 5.7. This makes it possible to analyse a ½-part of the model. As there also is an almost perfect symmetry for the ½-model, a ¼-model will also be analysed. There is though some problem in defining the symmetry boundary conditions for this ¼-model, when it is to be compared to the full model. How this is handled is later described in section 6.4.

The purpose of doing analyses with the smaller geometry is to see if it gives reasonable results compared to the full model, as this model is less time consuming.

6.1 Geometry and mesh

Alfa Laval provided the geometry of the model. It was generated by means of a CAD-software and saved as igs-files. The igs-files were then imported to ANSYS. The meshes for the two models are shown in Figure 6.1 and 6.2.

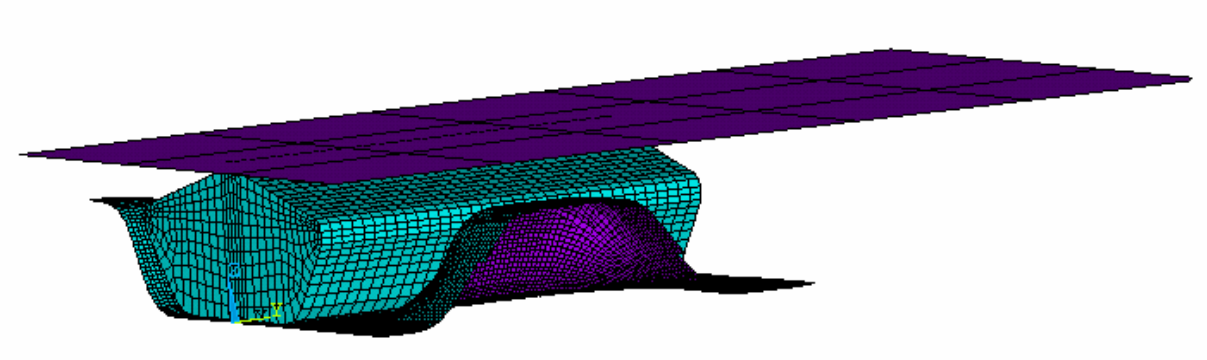

Figure 6.1: *The ½-model.*

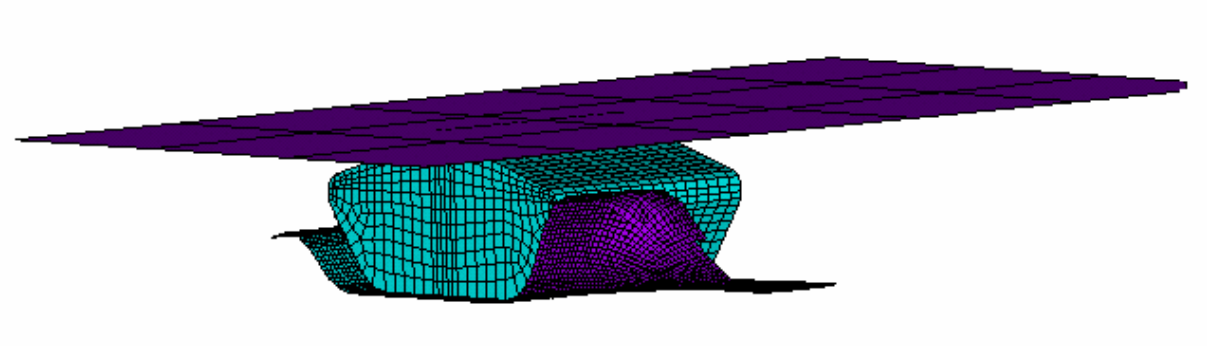

Figure 6.2: *The ¼-model.*

To create the mesh, the cross section area of the model was divided into smaller regions. The edges surrounding these regions were also divided into smaller parts. With these conditions ANSYS meshed the cross section area of the model, see Figure 6.3. By dividing the model into smaller regions, a better control of the mesh is given. Regions with a lot of activity can therefore be given more elements, whereas other regions can have a more course mesh. A fine mesh with a lot of elements gives a better accuracy than a coarse mesh, but is on the other hand very expensive in terms of CPU time. It is therefore important to create a mesh that has a reasonable CPU time and also yields a satisfying accuracy.

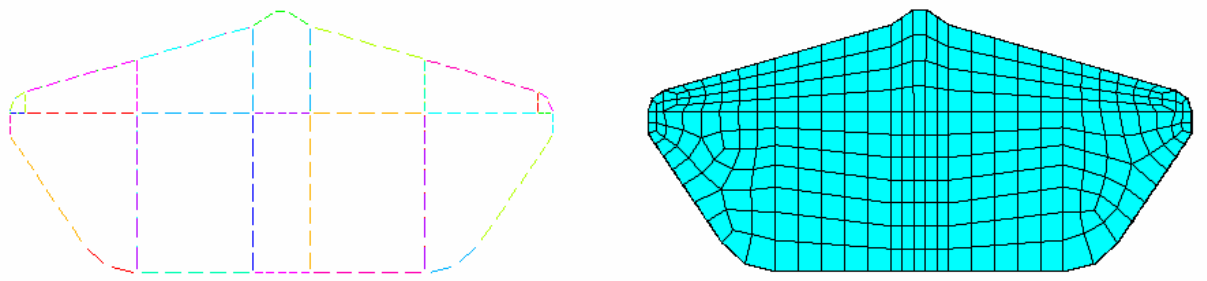

Figure 6.3: *The cross section area divided into small regions to the left and the generated mesh to the right.*

6.2 Choice of element

There are three different kind of elements used in the ANSYS model. A solid 3-D element type is used for the gasket. The corrugated- and horizontal plates are considered to be rigid bodies. They are therefore assigned a so called target element, which controls the contact with the gasket. The contact surface of the gasket is modelled by so called contact elements. The different types of elements will in the following be described.

6.2.1 Continuum element

The model of the gasket described in this project is a solid 3-D model. Suitable elements in ANSYS for these kinds of problems are SOLID 185, which is defined by eight nodes having three degrees of freedom at each node, namely translation in the nodal x-, y- and z-direction. SOLID 185 is a lower-order element, which means that it does not contain any midside nodes. The element has plasticity, hyperelasticity, stress stiffening, creep, large deflection and large strain capabilities. It also has capability for simulating deformations of nearly incompressible elastoplastic materials and fully incompressible hyperelastic materials. Therefore SOLID 185 makes a suitable element for the approach of this project.

6.2.2 Contact element

The gasket will under the simulation come in contact with the two plates. Therefore, contact elements have to be applied on the surface of the body. ANSYS uses a contact element called CONTA174. The element is applicable to 3-D structural and coupled field contact analyses. It has the same geometric characteristics as the solid element face with which it is connected to.

6.2.3 Target element

The two plates that come in contact with the gasket are defined as target surfaces. When the two plates are defined as rigid bodies in the issue of contact, they are modelled with target elements. The target elements used in these simulations are called TARGE170. They are used to present various 3-D target surfaces for the associated contact element CONTA174.

6.3 Contact

Problems involving contact can be defined in two groups, depending on the difference between the two contact body's stiffness. When the difference is large, the one with a higher stiffness can be treated as rigid and the other one as flexible. When the stiffness is more similar to each other the bodies can both be treated as flexible. Therefore, the two groups are called *rigid-to-flexible* and *flexible-to-flexible*. In this project, with a thick aluminium block and the rubber gasket, the contact is treated as rigid-to-flexible. Contact can in ANSYS be established by three different types, *surface-to-surface*, *node-to-surface* and *node-to-node*. Regardless of the type, one part is always modelled as target and the other one as contact. For rigid-to-flexible the rigid part is always modelled as the target. The contact was built up between body-surfaces, so called surface-to-surface provided by ANSYS. The advantage of using this method is that the exact location of contact does not need to be known before starting the simulation.

ANSYS provides several algorithms for dealing with contact problems, each with their different advantage. Only the one used in the project will here be presented. This algorithm is called, *the augmented Lagrangian method* (ALM), and is the default method for handling contact in ANSYS. This method is based on the algorithm called *Penalty method* (PM), which uses a spring to enforce the contact. ALM is an iterative series of penalty methods. The ALM algorithm is usually better and less sensitive than the PM. The spring is only active when two surfaces are in contact with each other, and to generate a contact force it is necessary that the target element penetrates the contact element a little bit.

For contact to be considered between two elements, the target element must be within a certain region of the contact element. This region is in ANSYS defined by the so called *Pinball Region*, which for 3-D cases is defined by a sphere. In reality a penetration does not exist and therefore the goal is to minimize the penetration under a specified tolerance, by use of high contact stiffness. There is a problem with defining a too high stiffness and a tight penetration tolerance, because it could lead to convergence problem. Contact problem including friction have a tangential force, which also is modelled by a spring. ANSYS uses the stiffness of the contact body to calculate proper normal contact stiffness. As for the tangential stiffness, the friction coefficient is also included. The stiffness values for controlling the contact can be factorized by the user in order to achieve a converged solution. They can also be defined as an absolute value. ANSYS recommends that the default settings should be used, as they are suitable for most contact problems.

For the solving procedure there are a few things to keep in mind to get an accurate and efficient solution. For contact problem, the Full Newton-Raphson solver should be selected and small "time" increment should be used to capture the real course of event. The Line Search tool is preferable to use if large deflection is assumed. This tool will help to stabilize the solution. When contact problem includes friction the solution gets more complicated, this due to that the stiffness matrix becomes unsymmetrical. ANSYS therefore uses a symmetrization algorithm so the default symmetric solver can carry out the solution. There is an unsymmetrical solver provided if problems with the convergence rate occur.

6.4 Boundary condition

The boundary condition is applied for avoiding rigid body motion, and also to take advantage of the symmetry in the model. The boundary condition for the gasket was to constrain displacement in its direction of length. For both models the two plates were constrained with zero displacements on the nodes in all directions, accept for the upper plate that was movable in the vertical direction so the deformation of the gasket could occur.

¼-model

The reason for trying the ¼-model was to see if it could give reasonable results, with a reasonable analyse time. With this model, two different kinds of boundary conditions were tested, all concerning the constraining of the nodes at the gasket sides.

1. Both sides are constrained.
2. Only one side is constrained and the other one is free to expand.

The results from ¼ - model are converted to fit the full model, in order to compare it with the experimental test results. A third “boundary condition” is also established. This is made with a combination of 1 and 2. Two models of 1 represent the middle of the gasket and two models of 2 represent the outer sides of the model. The result for this combination is also converted in order to compare it with the experimental tests.

½-model

This model has a real symmetry section, and is therefore just constrained at one side in its direction of length. At the other side, the nodes are free to move in all directions. The constrained side represent the mid cross section of the gasket in a full model. The result is converted to fit the experimental test results.

6.5 Load

For both models, ¼ and ½, the load was applied as a downward displacement of the upper rigid plate. This displacement started with the upper plate precisely over the gasket and ended just before contact appeared between the two plates. The distance for the displacement was measured before the analysis. The nodes at the upper plate had this displacement in the vertical direction as a form of boundary condition. In the solving procedure this total displacement was divided into increments and applied step by step until the total displacement was reached. The size of these increments varied during the analysis so the solution always converged in each load step. The user defines the range where the increment can vary, this by deciding a start-, max- and min increment which all are defined as a fraction of the total displacement.

Chapter 7

FE-analyses and results

In this chapter the results from FE-analyses for geometry 1 will be discussed. The results from the different tests made will be described one by one, starting with the ¼-model.

7.1 ¼-model

As mentioned earlier, the ¼-model, see Figure 6.2 is made in order to investigate the accuracy of such a small model. The different boundary conditions are described in chapter 6.

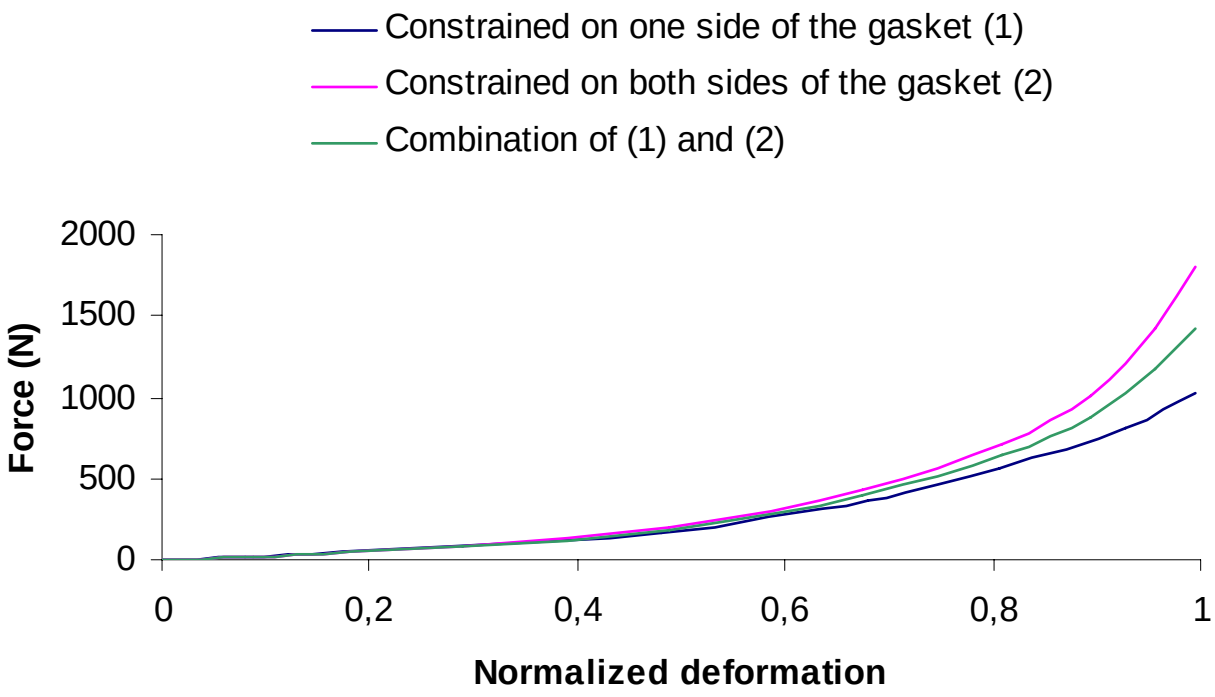

Figure 7.1: *Force-deformation curves for the different boundary conditions, for the ¼-model*.

Commentary

The results that can be seen in Figure 7.1, shows what could be expected. The model becomes stiffer the more constrained it is. The two boundary conditions, (1) and (2), represent a too stiff- and a too weak model. It is therefore reasonable to believe that the curve for the ½-model will be in between these two curves. The question that remains is if the combination will be a good approximation for the ½-model. This will be investigated in the next section.

The major difference between the tests shows the importance of choosing boundary conditions carefully.

7.2 Comparison between the ½- and ¼-model

In this chapter a comparison between the two models will be evaluated. All of the different combinations for the ¼-model are compared to the ½-model.

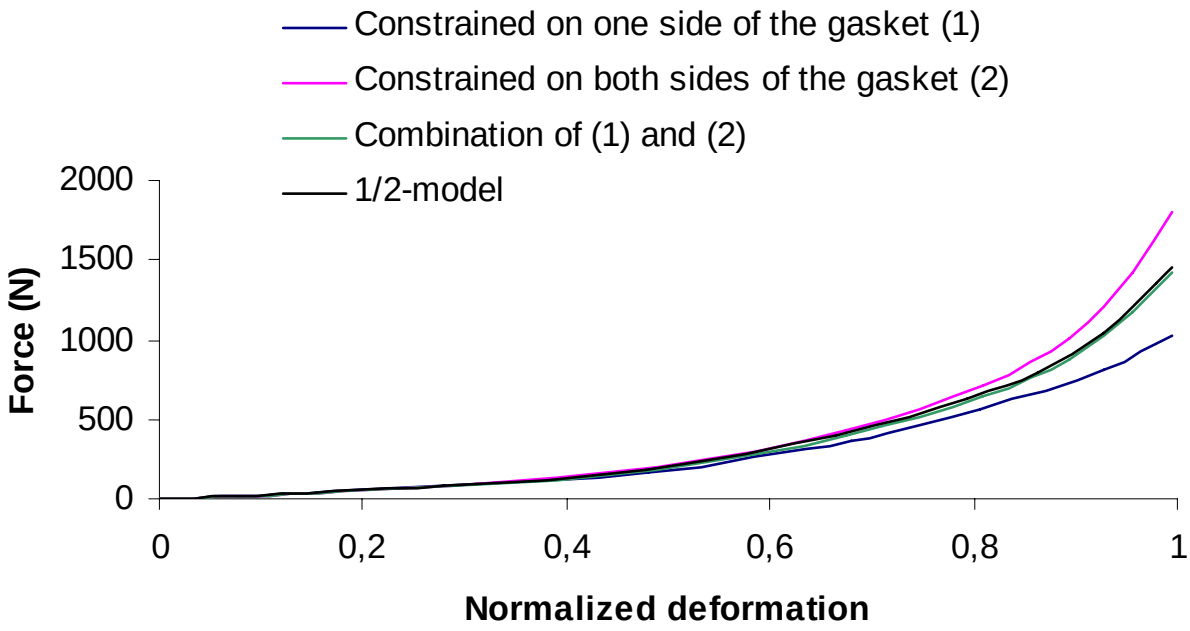

Figure 7.4: *Comparison of the results for ½- and ¼-model*.

Commentary

The results can be seen in Figure 7.4. As expected, the curve for the ½-model is between the curves for the two ¼-models. The combination of the two boundary conditions seems to be a good approximation of the ½ -model. One should although be careful when doing such an approximation, it might just be good for this analysis. If this combination holds as a good combination will later be investigated with geometry 2, for both gasket materials NBR and EPDM in chapter 9.

7.3 Position dependency for the gasket

In this section the dependency of the gaskets position will be evaluated for the ½-model, as described in chapter 5, this could affect the result in the tests. Three analyses have been performed and the positions of the gasket are illustrated in Figure 7.2.

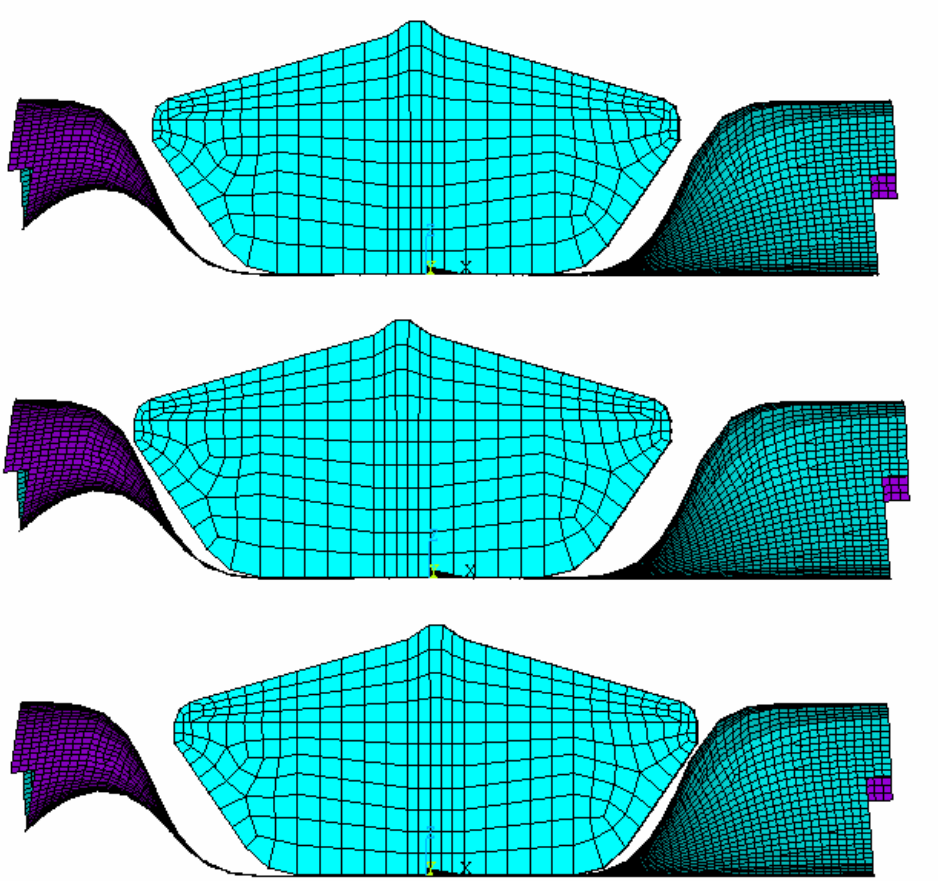

Figure 7.2: *The three different positions for the gasket. Centre-, left- and right-orientated.*

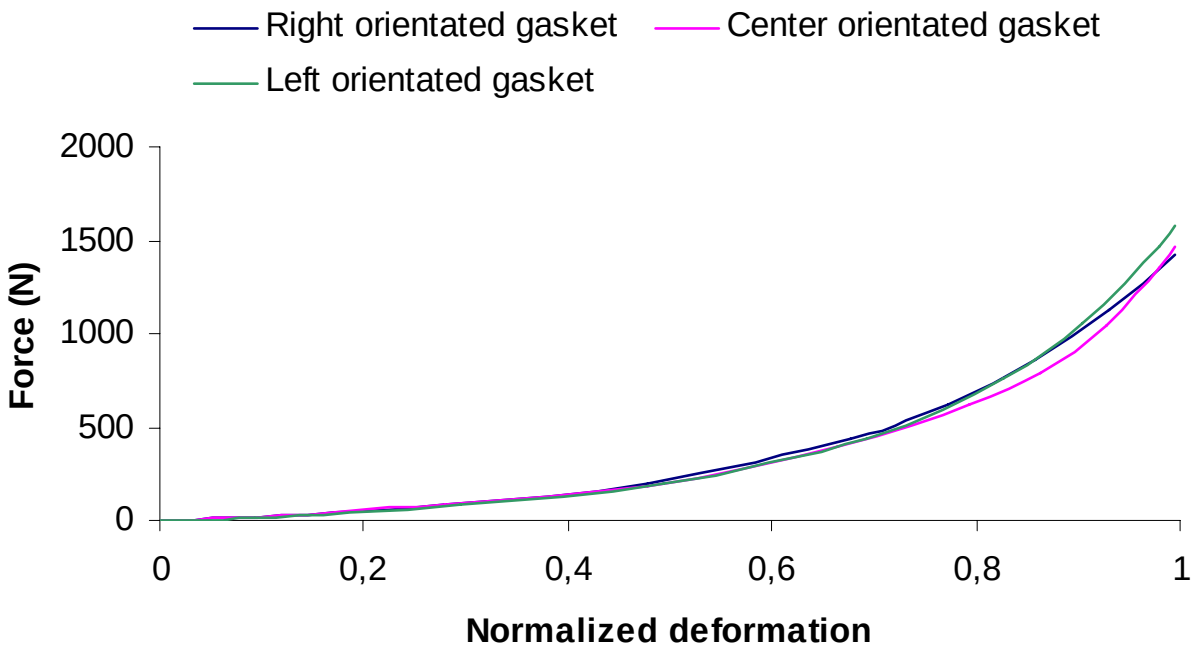

Figure 7.3: *Force-deformation curves for the different gasket placement, for ½-model.*

Commentary

The results are shown in Figure 7.3. As can be seen, there are no major differences in the results, but still the placement of the gasket affects the result in some way. The right- and left-orientated gasket shows a higher force than the centre-orientated. The reason for this is that the gasket is restricted by the plate to deform less free than the centre-orientated. In the end of the deformation, the right- and centre-orientated gasket show the same force, which can be explained by the fact that the centre-orientated gasket also becomes restricted by the plate. As can be seen in Figure 5.7, the plate restricts the left-orientated gasket to deform almost completely in the left direction. This is the reason for the left-orientated gasket to have the highest force.

The left-orientated model had difficulties to converge, which made it necessary to have a lower value of the factor for the parameter controlling the contact stiffness. This could lead to a lower force, and it is therefore important that the factor is as high as possible. This has not been investigated further.

Chapter 8

FE-results vs. experimental tests

In this chapter a comparison between the FE-analyse and the tests made at Alfa Laval and LTH will be made for geometry 1, with NBR as gasket material. The results from the FE-analyses are the centre-orientated ½-model used in ANSYS. The plots for the experimental results from Alfa Laval and LTH are here just added with the FE-results.

8.1 Experiments at Alfa Laval

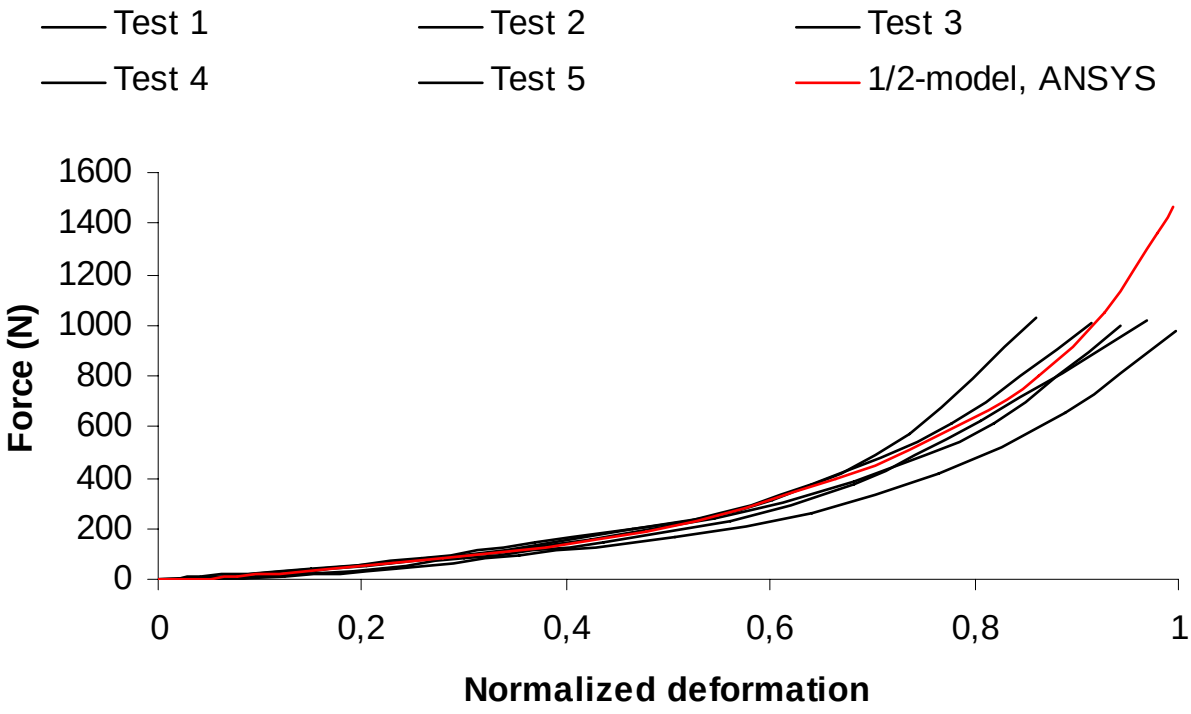

Figure 8.1: *FE-analysis compared to tests made at Alfa Laval for geometry 1 (NBR).*

Commentary

The results from the tests made at Alfa Laval have a wide spread, as described earlier. However, test 2, 3 and 4 shows a fairly good resemblance to the FE-analysis. As mentioned earlier about the problems with the deformation for the tests at Alfa Laval, it is not possible to reach the same deformation as in the FE-analysis. It is therefore only possible to compare the results up to a certain level of deformation. As Alfa Laval is interested in the reaction force of the gasket when the plates of the PHE are nearly in contact with each other, the equipment is not sufficiently good enough. With this conclusion and earlier discussed sources of error in mind, no further comparing between FE-analysis and tests at Alfa Laval will be made.

8.2 Experiments at LTH

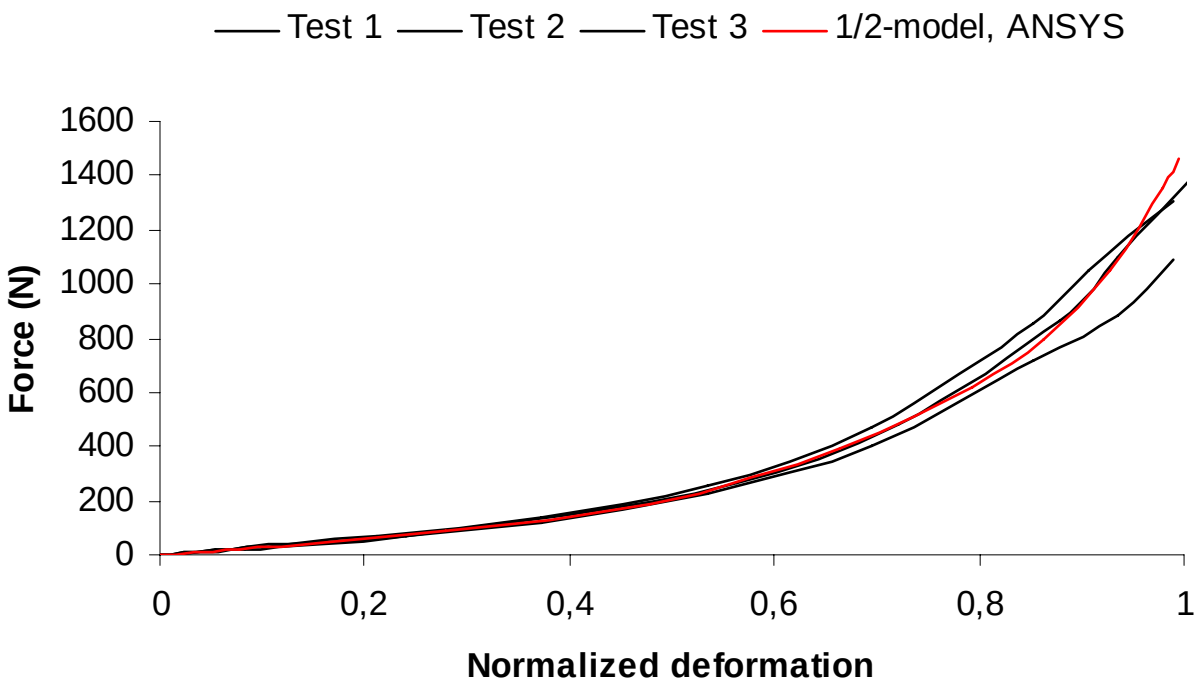

Figure 8.2: *FE-analysis compared to tests made at LTH for geometry 1 (NBR).*

Commentary

The tests made at LTH are almost compressed to the desired deformation, this due to the circumstances described in chapter 5. The FE-analysis shows good resemblance compared to test 1 and 2. The differences between these two tests and the FE-result can be explained with the earlier mentioned sources of error, such as the placement of the gasket as well as the difficulty of finding the starting point of the deformation. Another explanation can also be that the material model used in the FE-analysis include Mullin's effect and therefore is a little bit softer. The disagreement for test 3 (the lower black curve) at the end of deformation can not be explained and it is desirable to have more tests. This could unfortunately not be done, due to the lack of time.

It is noted that the FE-model becomes much stiffer than the experimental tests at the end of the deformation process.

Chapter 9

FE-analyses for geometry 2

The purpose of this chapter is to evaluate if the modelling procedure for geometry 1 also can be made for geometry 2. The gasket material analysed for geometry 2 is NBR and EPDM. In section 9.1 the ¼-model and the ½-model are compared to each other to see if the combination of the ¼-model, described in chapter 6, gives a reasonable result.

Section 9.2 will compare the ½-model to the experimental tests performed at LTH, for both NBR and EPDM. The plots for the experimental results from LTH are just added with the FE-results.

It should be mentioned that the ½-model with NBR as gasket material did not reach the desired deformation in ANSYS, due to difficulties in convergence. Even though a higher mesh density was used, the problem still occurred. Therefore, the experimental test will be compared to the model that gave the largest deformation. By constraining the ½-model in both ends, the solution had no problem in converging. Therefore the free end should be ascribed to be the reason for the convergence problem.

9.1 ¼-model vs. ½-model

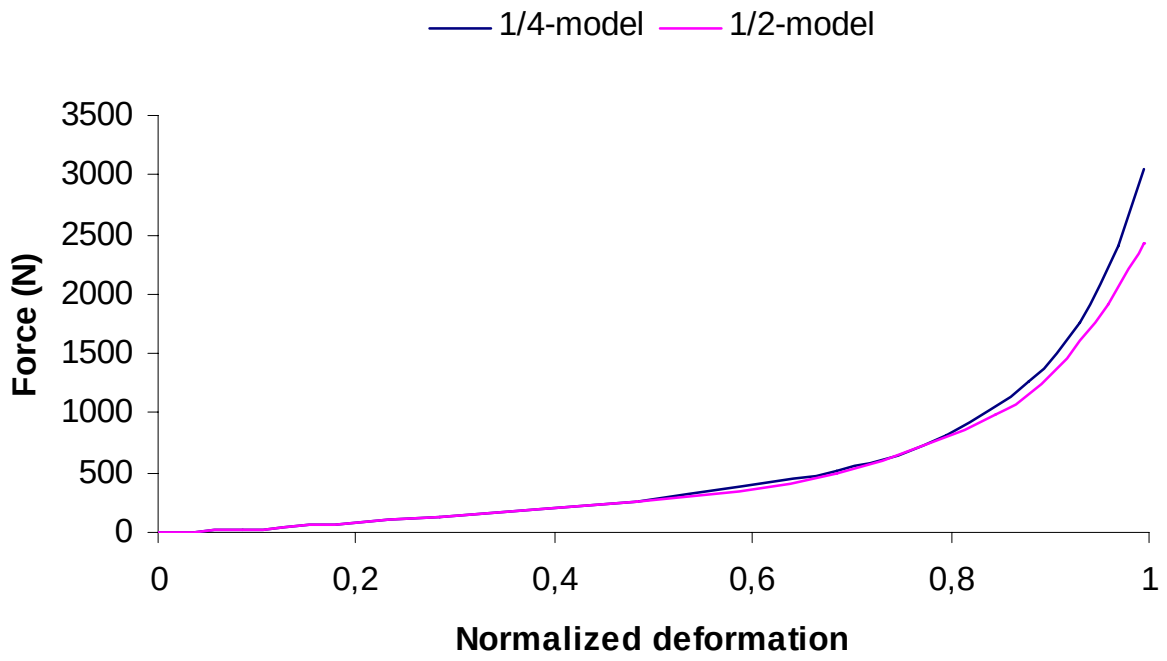

Figure 9.1: *Comparison between ¼- and ½-model with geometry 2 (EPDM)*

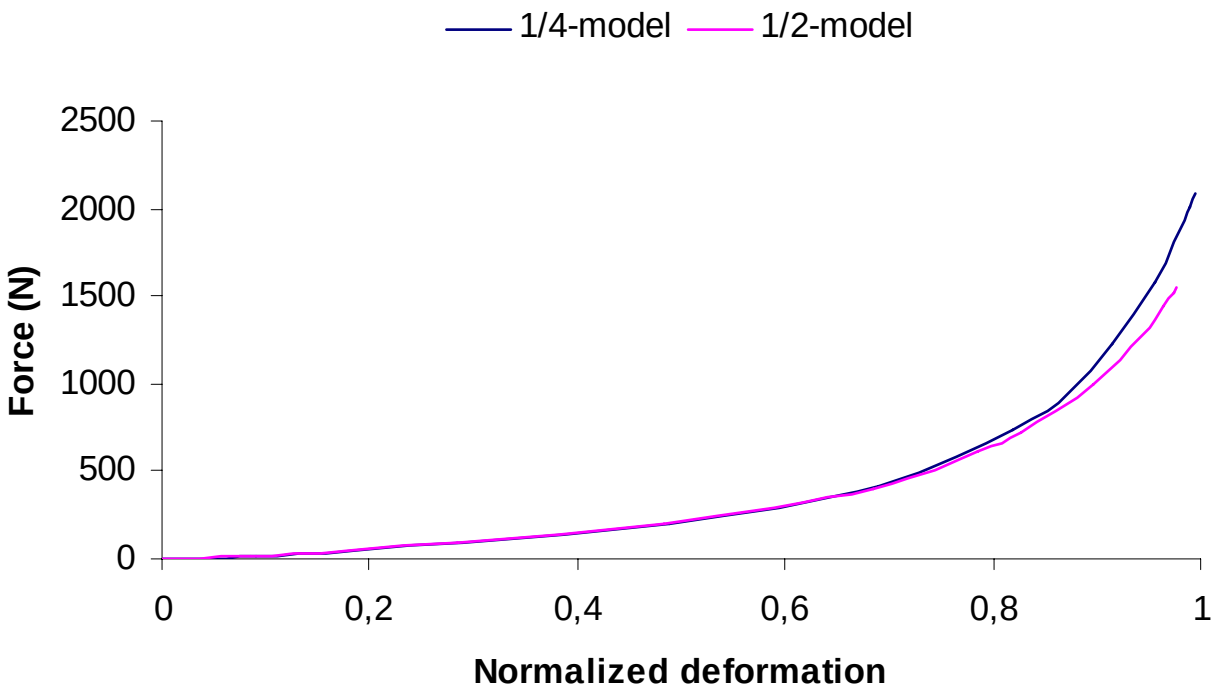

Figure 9.2: *Comparison between ¼- and ½-model with geometry 2 (NBR).*

Commentary

For both EPDM and NBR the combination of the ¼-model give stiffer results than the ½-model in the last section of the deformation. For the deformation up to 80 %, the ¼-model gives a reasonable result. The explanation for the difference in the last 20 % of the deformation might be that the gasket then starts to deform more dependently on the geometry of the corrugated plate. In the Figures 9.3 and 9.4 the deformation near 80% and 100% are shown, and in Figure 9.5 the results for the two ¼-models and the ½-model are compared. It could be seen in Figure 9.5 that the results dramatically starts too differ when the gaskets deforms against the corrugated plate.

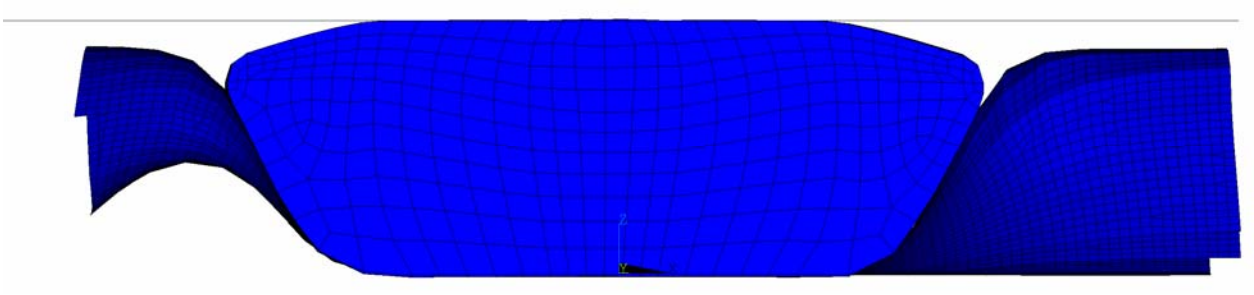

Figure 9.3: *80 % of the deformation for the ¼-model, NBR, with both constrained ends.*

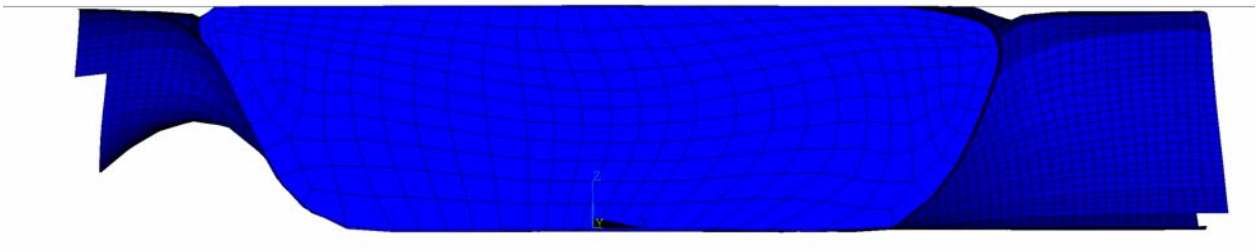

Figure 9.4: *100 % of the deformation for the ¼-model, NBR, with both constrained ends.*

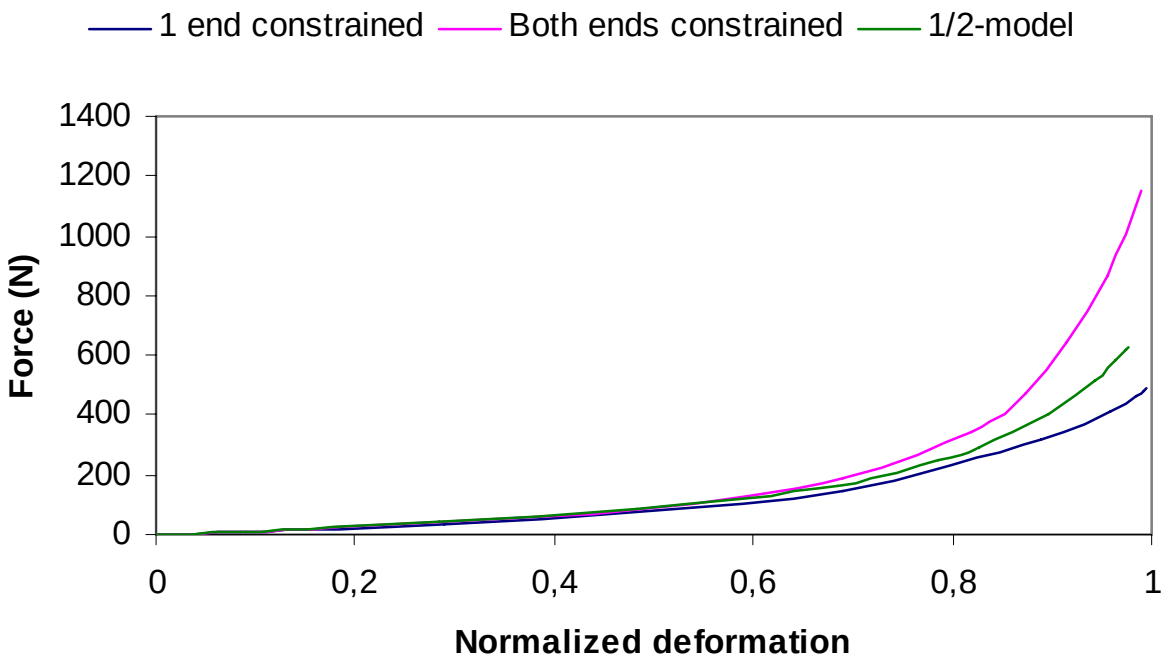

Figure 9.5: *Three force-deformation curves for ¼-model, with one end constrained and the other with both ends constrained, and ½-model. The results from ¼-models are extrapolated to the length of the ½ -model. The material is NBR with geometry 2.*

9.2 FE-model vs. experimental tests at LTH

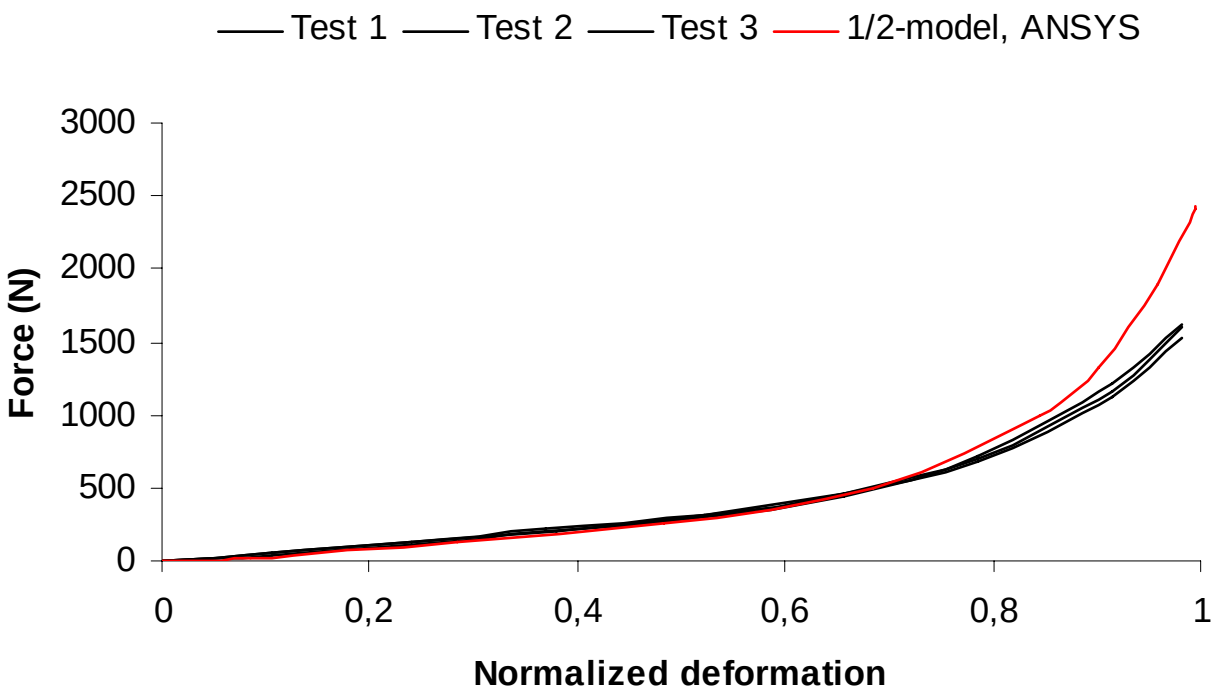

Figure 9.6: *Comparison between the ½-model and the experimental tests for geometry 2 (EPDM).*

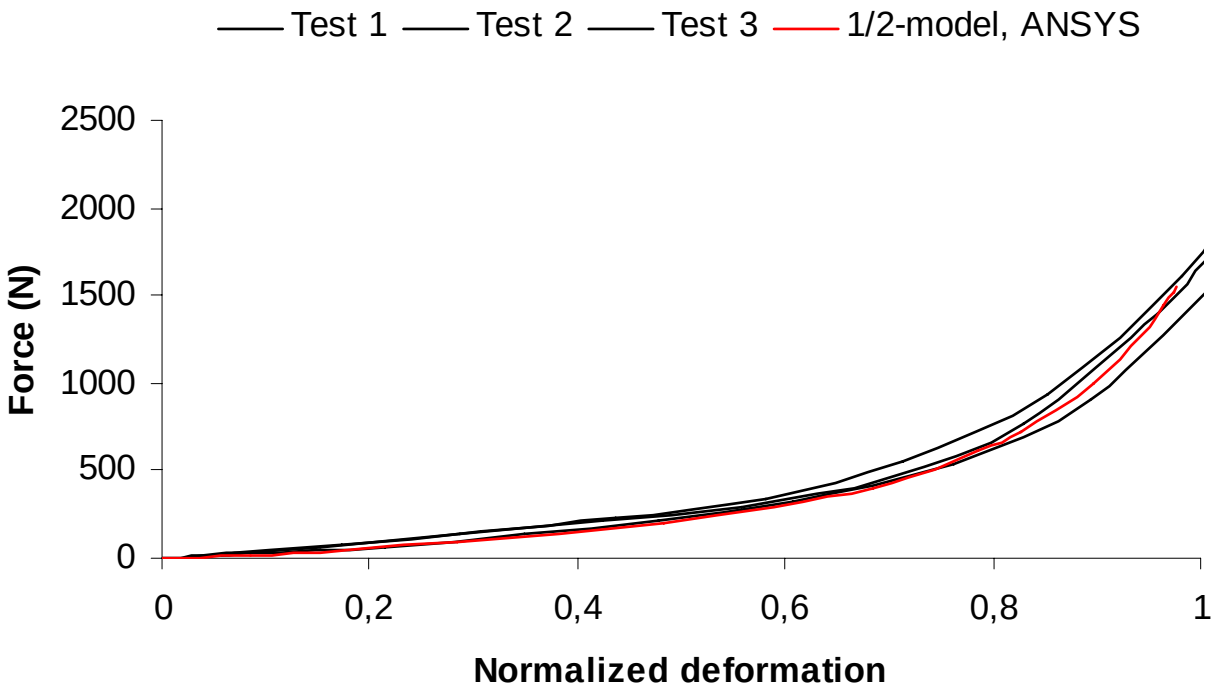

Figure 9.7: *Comparison between the ½-model and the experimental tests for geometry 2 (NBR).*

Commentary

For both NBR and EPDM, the FE-results show a good alignment with the experimental results up to a certain level of compression. The FE-model becomes stiffer at the end of the procedure, which for EPDM is very drastic. This affect have also appeared for geometry 1. The problems occur at the deformation level when the gasket starts to deform against the sides of the corrugated plates and becomes more and more enclosed. As earlier mentioned, an assumption was made that the plates can be considered as rigid bodies. If the plates had been defined as flexible bodies, the stiffened behaviour at the end of the deformation process might have been reduced. The Yeoh-parameters are evaluated from shear tests, see Appendix A, which might not be fully representative for the problem in this project when compression is made, and can be another explanation to the problem. Therefore the conclusion is that the plates should be considered flexible and that the Yeoh-parameters can not fully represent this state of deformation.

Chapter 10

Concluding remarks

10.1 Conclusion

In this project, different tests have been carried out, both experimental as well as analytical. To begin with the experimental tests performed at Alfa Laval, the results show an uncertainty as the results are spread in a wide range. As the upper block is horizontally un-balanced, as well as the poor accuracy of using feeler gauges, the deformation of the gasket is difficult to measure. As this test equipments main purpose is to calibrate a load cell, it has to be substantially improved for these kinds of purposes.

The tests performed at LTH gave more equivalent force-deformation curves, although there were some differences between the tests. More tests would have been desirable, but due to the lack of time it was not possible to perform any more tests than the ones made.

Tests at Alfa Laval showed that the relaxed force depends on the speed of deformation for the gasket. This was therefore also tested at LTH, but no such behaviour was noticed. As this was not in the range of the project, no further investigation was made.

ANSYS is able to handle problem for hyperelastic material models. There were problems for ANSYS to handle geometry 2 with NBR as gasket material and this was not fully investigated, but as the model worked when both ends were constrained, the problem at hand is ascribed to the free end. Further improvement on the model must be made to solve this problem. The FE-model shows good comparison with the tests up to a certain level of deformation. When the gasket is getting enclosed by the plates the FE-model becomes much stiffer than the tests. The reason for this behaviour can be that the plates are considered rigid and Yeoh-parameters used in this project are evaluated from shear tests, which might not fully represent the compression process. The Yeoh-parameters fits well in the beginning and it is possible that they are not well calibrated for the large straining that occurs.

The use of the ¼-model, with the assigned boundary conditions cf. chapter 6, gives very good results compared to the ½-model, especially for geometry 1. Even for geometry 2 the results shows good agreement to the ½-model until the gasket starts to deform more dependently on the sides of the corrugated plate. This distance in compression is the same as when the FE-model became stiffer than the tests, which make the use of the ¼-model a good indicator of the behaviour for the forces up to that specific level of compression.

Alfa Laval does not want to be too conservative when calculating the gasket force. As just mentioned the model in this project with rigid bodies and given Yeoh-parameters becomes stiffer than the tests at the end of the deformation process, which gives some conservatism in the reaction force.

10.2 Future work

This project was the initial step in the creation of a gasket table that will be used in the designing process of plate heat exchangers. As a suggestion, the next step is to perform experimental test with the same test objects as used in this project, but with constrained ends.

The reason for this is that those tests could be compared with FE-analyses, which are performed in the way they will be in the future when analysing a PHE. Before this is done, FE-analyses with flexible bodies should be carried out and an investigation concerning the Yeoh-parameter is necessary, and how to handle the problems that occur when the gasket becomes enclosed.

Alfa Laval's test equipment is today not reliable for the use of this kind of projects, due to the problems mentioned in chapter 5. The necessary improvements are to stabilize the upper block so a homogeneous deformation is achieved and also to have better equipment for measuring the deformation. As is seen from the experimental tests, especially in Figure 5.12, the maximal reaction force is dependent on the velocity of deformation. When the plate heat exchangers are manufactured it is of interested to know how fast it could be assembled and thereby ensures that no failure and possible accident occurs. With improved test equipment that also can control the velocity of deformation, important information for the assembling process can be obtained.

The test at Alfa Laval showed that the velocity of deformation affected the relaxed force, but the phenomenon was not found in the tests at LTH. Better test specimens and more tests with reliable equipment is desirable for further investigation in this case.

References

[1] Alfa Laval, Booklets

[2] ANSYS, Inc. Theory Reference, Vol 10, 2005.

[3] Austrell P.-E., (1997), *Modeling of Elasticity and Damping for Filled Elastomers*, Report TVSM-1009, Lund University, Division of Structural Mechanics, Sweden 1997.

[4] Austrell P.-E., Bellander M., Carlsson U., Kari L., Persson S., Stenberg B., (1998), *Survey of Design Methods and Material Characteristics in Rubber Engineering*, Report TVSM-3036, Lund University, Division of Structural Mechanics, Sweden 1998.

[5] Holzapfel G.A., (2000), *Nonlinear Solid Mechanics, a Continuum Approach for Engineering*, Wiley, Chichester, England 2000.

[6] Krenk S., (2005), *Non-linear Modelling and Analysis of Structures and Solids*.

[7] Nilsson C., (2003), *FE-analysis of a Plate Heat Exchanger Gasket*, Report TVSM-5118, Lund University, Division of Structural Mechanics, Sweden 2003.

[8] Ottosen N.S., Petersson H., (1992), *Introduction to the Finite Element Method*, Prentice Hall, Europe 1992.

[9] Sundström B., (1999), *Handbok och Formelsamling i Hållfasthetslära*, Institutionen för hållfasthetslära, KTH, Sweden 1999.

Appendix A

Yeoh-parameters

The parameters in the hyperelastic model are obtained from experimental data by a fitting procedure, described in this Appendix. These parameters have been carried out by Per-Erik Austrell and Erik Serrano, commissioned by Alfa Laval, with the use of a *simple shear* method. From the general constitutive law for a hyperelastic material, the relation between shear stress and shear strain will be calculated for this simple shear test. The procedure for calculating proper Yeoh-parameters from experimental test will also be described. For a more elaborate description, the reader is referred to [3].

A.1 Simple shear test

The constitutive law for a *hyperelastic and isotropic* material is derived in equation (4.40). In this test the material is assumed to be *incompressible*, reducing the third invariant, I_3. According to [5] the constitutive law takes the form,

$$\sigma = 2(\frac{\partial W}{\partial I_1} + I_1 \frac{\partial W}{\partial I_2})\mathbf{B} - 2\frac{\partial W}{\partial I_2}\mathbf{B}^2 + p \cdot \mathbf{I} \tag{A.1}$$

where σ is the Cauchy stress tensor. $\mathbf{B} = \mathbf{F}\mathbf{F}^T$ is the left Cauchy-Green deformation tensor and *p* is the pressure stress defined as

$$p = \frac{1}{3}(\sigma_{11} + \sigma_{22} + \sigma_{33}) \tag{A.2}$$

With the deformation for simple shear seen in Figure A.1, the deformation gradient **F** is

$$\mathbf{F} = \begin{bmatrix} 1 & 0 & \kappa \\ 0 & 1 & 0 \\ 0 & 0 & 1 \end{bmatrix} \tag{A.3}$$

where $\kappa = \frac{\delta}{H}$ is called the *direct shear* strain.

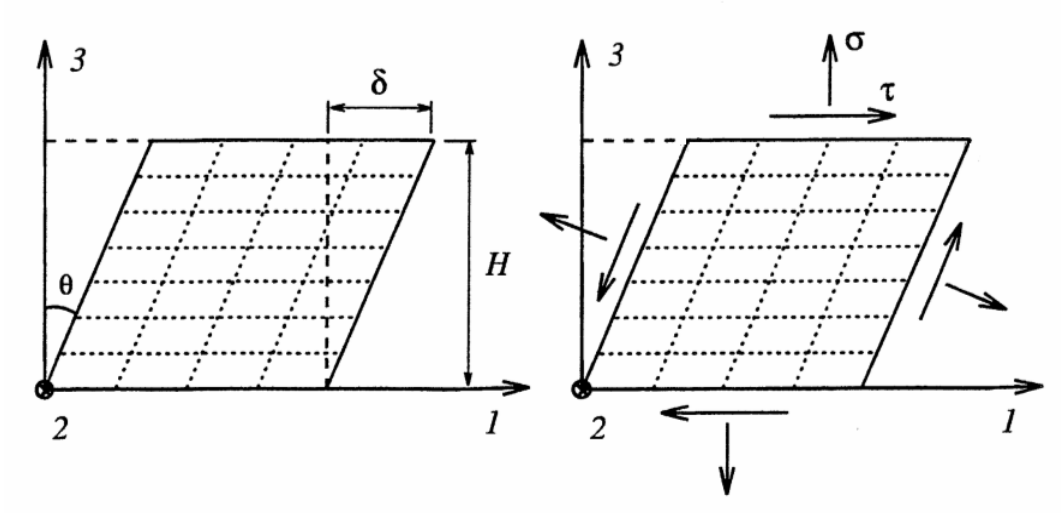

Figure A.1: *Simple shear test.* [3]

The strain invariants with simple share are

$$\begin{cases} I_1 = tr(\mathbf{B}) = 3 + \kappa^2 \\ I_2 = \frac{1}{2}(tr^2(\mathbf{B}) - tr(\mathbf{B})^2) = 3 + \kappa^2 \end{cases} \tag{A.4}$$

Inserting (A.3) and (A.4) into (A.1) yields

$$\begin{bmatrix} \sigma_{11} & \sigma_{12} & \sigma_{13} \\ \sigma_{21} & \sigma_{22} & \sigma_{23} \\ \sigma_{31} & \sigma_{32} & \sigma_{33} \end{bmatrix} = 2\left(\frac{\partial W}{\partial I_1} + (3+\kappa^2)\frac{\partial W}{\partial I_2}\right)\begin{bmatrix} 1+\kappa^2 & 0 & \kappa \\ 0 & 1 & 0 \\ \kappa & 0 & 1 \end{bmatrix} - 2\frac{\partial W}{\partial I_2}\begin{bmatrix} 1+3\kappa^2+\kappa^4 & 0 & 2\kappa+\kappa^3 \\ 0 & 1 & 0 \\ 2\kappa+\kappa^3 & 0 & 1+\kappa^2 \end{bmatrix} + p\begin{bmatrix} 1 & 0 & 0 \\ 0 & 1 & 0 \\ 0 & 0 & 1 \end{bmatrix} \tag{A.5}$$

The only shear stress different from zero is $\tau = \sigma_{13} = \sigma_{31}$, which is obtained as,

$$\tau = 2\left(\frac{\partial W}{\partial I_1} + \frac{\partial W}{\partial I_2}\right)\kappa \quad \text{with} \quad \kappa = \frac{\delta}{H} \tag{A.6}$$

The shear stress for the Yeoh model (4.47), becomes

$$\tau^{teor} = 2(C_{10} + 2C_{20}\cdot\kappa^2 + 3C_{30}\cdot\kappa^4)\kappa \tag{A.7}$$

A.2 Least squares fit to test data

Figure A.2 shows the experimental data points from the shear test and the fitted curve for the corresponding Yeoh-model based on the data points. The circles are the different data points evaluated from the test.

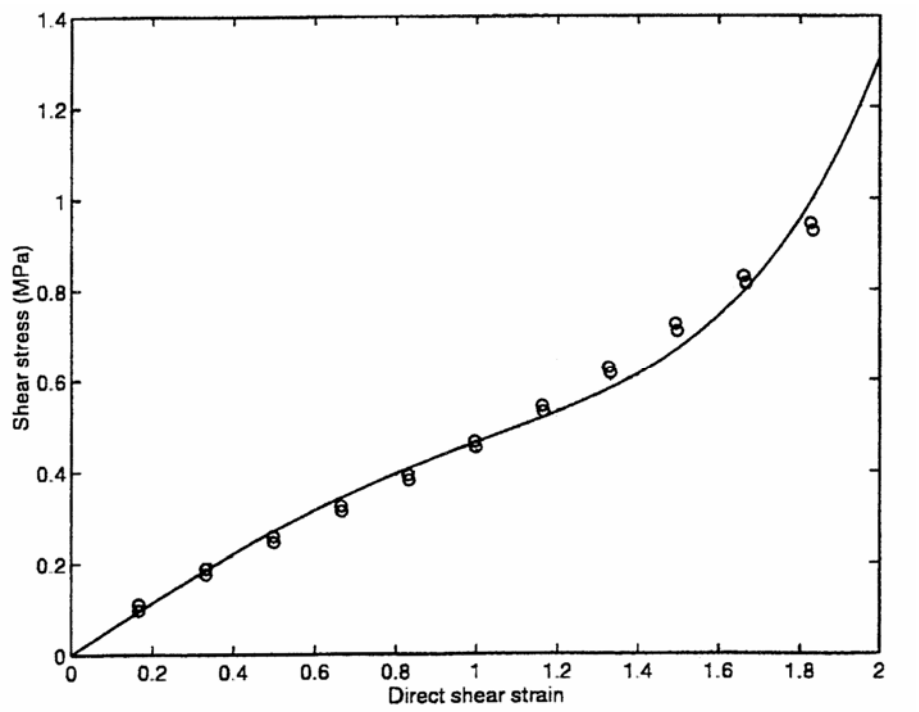

Figure A.2: *Fit of the Yeoh-model to experimental test.*[3]

With the experimental test it is possible to evaluate the Yeoh-parameters, with the use of the constitutive model, cf. (A.7). It is desirable to get a good agreement between the theoretical and experimental values,

$$\tau_i^{teor} \approx \tau_i^{\exp} \tag{A.8}$$

To get proper values of the constants in the Yeoh-model it is desirable to have many experimental data points within the range of interest. With the different shear stress- and stretch values a linear system of equations can be written as

$$\mathbf{Ac} = \mathbf{b} \tag{A.9}$$

As there are more than three data points from the experimental test, the equation (A.9) becomes overdetermined, as **A** is an nx3 matrix corresponding to the *n* experimental points, **c** is a 3x1 matrix with $c_1 = C_{10}, c_2 = C_{20}, c_3 = C_{30}$ and **b** is an nx1 matrix. To get the Yeoh-parameters, this overdetermined equation system must be treated to achieve a solution.

By inserting a trial solution $\mathbf{c}^*$ in (A.9) a difference will yield between the left- and right-hand sides. A residual **e** is expressing the difference as,

$$\mathbf{e} = \mathbf{Ac}^* - \mathbf{b} \tag{A.10}$$

which is a vector containing the relative error in each data point. The aim is to find a solution of $\mathbf{c}^*$ that minimizes the error. Therefore the size of the residual must be measured in some way, here represented as,

$$\left\|\mathbf{e}\right\|_2^2 = \mathbf{e}^T\mathbf{e} \tag{A.11}$$

This expression can be rewritten as,

$$\phi = \left\|\mathbf{e}\right\|_2^2 = (\mathbf{Ac}-\mathbf{b})^T(\mathbf{Ac}-\mathbf{b}) \tag{A.12}$$

To minimize the relative error between theory and experiment, equation (A.12) must be differentiated by **c**, giving

$$\frac{\partial\phi}{\partial c_i} = 0 \quad i = 1,2,...n \tag{A.13}$$

Index notation yields

$$\frac{\partial\phi}{\partial c_j} = \frac{\partial e_i^2}{\partial c_j} = 2e_j\frac{\partial e_i}{\partial c_j} \tag{A.14}$$

and

$$\frac{\partial e_i}{\partial c_j} = \frac{\partial}{\partial c_j}(A_{ik}c_k - b_i) = A_{ik}\delta_{kj} = A_{ij} \tag{A.15}$$

with these expressions (A.13) becomes

$$A_{ij}A_{ik}c_k = A_{ij}b_i \tag{A.16}$$

which can be written in matrix form as

$$\mathbf{A}^T\mathbf{Ac} = \mathbf{A}^T\mathbf{b} \tag{A.17}$$

Observe that (A.17) is an ordinary linear system of equations with the same number of unknowns as the number of equations, and from these equations the three parameters C_{10}, C_{20} and C_{30} can be calculated.

Appendix B

Fully constrained model

Geometry 2 with NBR as a gasket material had convergence problem when it only was constrained at one end, cf. chapter 9.2. When this model was constrained at both ends the problems with convergence disappeared. In this Appendix the result from this model will be compared to the ¼-model, also with both ends constrained. The reason for this comparison is that when a complete PHE is to be investigated only a short section of the gasket is desirable to analyse. To reduce analyse time, the smallest model possible is desirable. The ¼-model is an almost perfect symmetry of the ½-model, see Figure 5.7. It is therefore of interest for Alfa Laval to see if such a small model can be used for their future analysis. With these boundary conditions the gasket forces for the complete PHE is modelled in a realistic way. It is also desirable to perform experimental tests where the gasket ends are constrained at both ends, to show that the model agree with the reality.

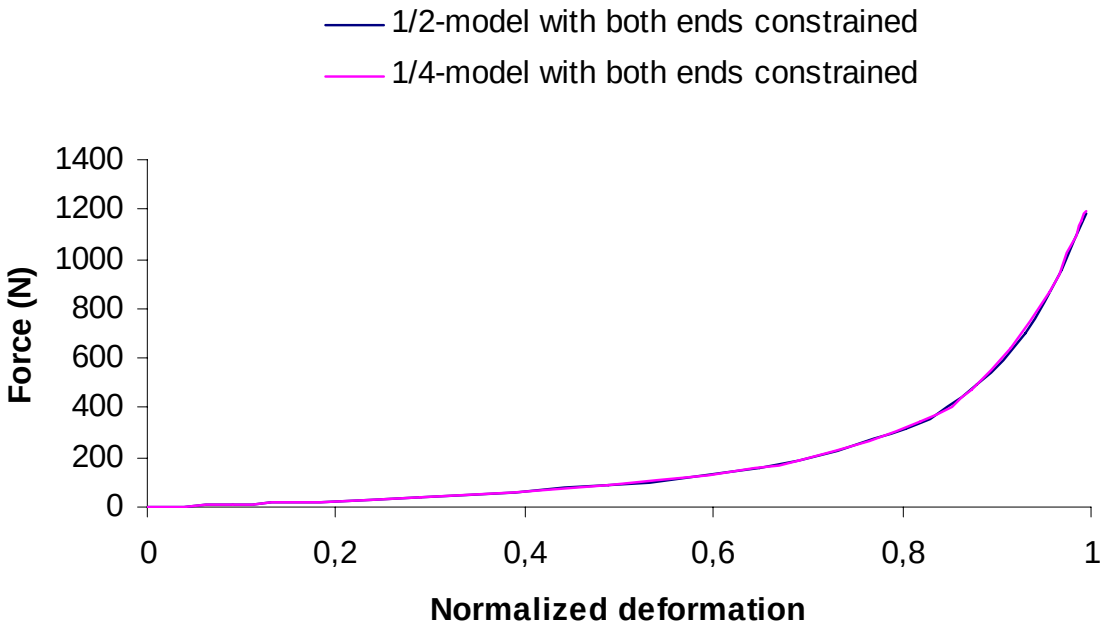

Figure B.1: *Comparison between ½- and ¼-model with both ends constrained. Geometry 2 (NBR).*

Commentary

As can be seen from figure B.1 the results show a very good agreement. This is not unexpected as the ¼-model is, as mentioned, an almost perfect symmetry model of the ½-model. The small difference between the two models does not give any effects in the results. The conclusion from this test is that is possible and desirable to perform analysis with the ¼-model.